

Detecting Contextual Hallucinations in Large Language Models with Frequency-Aware Attention

Siya Qi¹ Yudong Chen² Runcong Zhao¹ Qinglin Zhu¹ Zhanghao Hu¹ Wei Liu¹
Yulan He^{1,3} Zheng Yuan^{4,3} Lin Gui¹

Abstract

Hallucination detection is critical for ensuring the reliability of large language models (LLMs) in context-based generation. Prior work has explored intrinsic signals available during generation, among which attention offers a direct view of grounding behavior. However, existing approaches typically rely on coarse summaries that fail to capture fine-grained instabilities in attention. Inspired by signal processing, we introduce a frequency-aware perspective on attention by analyzing its variation during generation. We model attention distributions as discrete signals and extract high-frequency components that reflect rapid local changes in attention. Our analysis reveals that hallucinated tokens are associated with high-frequency attention energy, reflecting fragmented and unstable grounding behavior. Based on this insight, we develop a lightweight hallucination detector using high-frequency attention features. Experiments on the RAGTruth and HalluRAG benchmarks show that our approach achieves performance gains over verification-based, internal-representation-based, and attention-based methods across models and tasks.¹

1. Introduction

Large Language Models (LLMs) have achieved strong performance across many natural language processing tasks, yet they can produce *hallucinated outputs* that are fluent but not supported by the given input or external facts (Ji et al., 2023; van Deemter, 2024). This issue is especially

¹Department of Informatics, King’s College London, UK
²Department of Statistics, University of Warwick, UK ³The Alan Turing Institute, UK ⁴School of Computer Science, The University of Sheffield, UK. Correspondence to: Lin Gui <lin.l.gui@kcl.ac.uk>, Siya Qi <siya.qi@kcl.ac.uk>.

Preprint. February 23, 2026.

¹Code and data are available at <https://github.com/siyaqi/FrequencyAwareHallucination>.

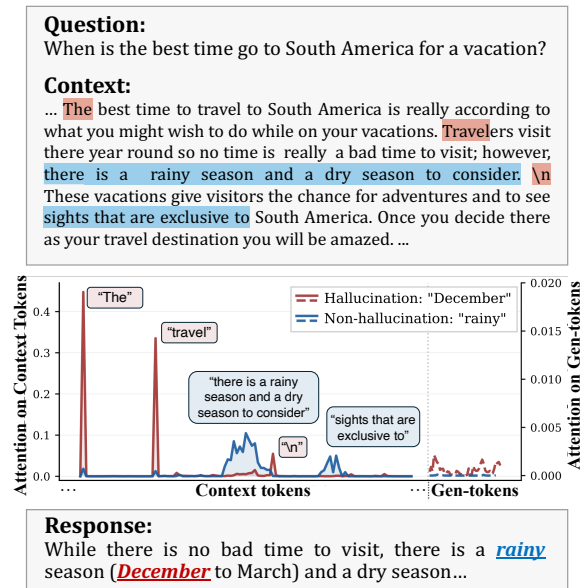


Figure 1. Attention weights over context and previously generated tokens for a grounded token (blue, “rainy”) and a hallucinated token (red, “December”) in a context-based QA example.

pronounced in the **context-based generation** settings, such as the summarization task, where models are explicitly expected to ground in a provided source context (Hu et al., 2024a). Therefore, effective hallucination detection is essential for building trustworthy language systems and enabling downstream mitigation strategies.

A common approach to hallucination detection verifies model outputs against the source context, for example, using semantic similarity measures or LLM-as-a-judge frameworks (Kryscinski et al., 2020; Laban et al., 2022; Manakul et al., 2023). Such methods compare the output with contextual evidence and are applied post hoc, rather than reflecting the model’s generation dynamics. Motivated by this limitation, recent work has explored hallucination detection from intrinsic signals available during generation, including token

probabilities, hidden representations, and attention patterns (Sun et al., 2025; Chen et al., 2024; Chuang et al., 2024a). Among these signals, attention is particularly informative, as it directly reflects how the model allocates content focus during generation (Wiegrefe & Pinter, 2019). Prior studies have shown that hallucinated generations are often associated with unstable or diffuse attention behavior (Feng et al., 2023a; Gong et al., 2024; Sriramanan et al., 2024). However, *how to quantify attention stability or uncertainty remains an open problem.*

Most existing attention-based methods summarize attention using coarse statistics, such as attention mass, entropy, or transition patterns (Huang et al., 2025; Sun et al., 2025; Chuang et al., 2024a). While effective at capturing overall concentration, such scaling-based metrics often discard fine-grained sequential variation. For example, in Figure 1, we prompt LLaMA-2-7B-Chat with a context-based question and require the model to answer strictly using the provided context. Although most generated tokens align well with the source, the model produces a hallucinated token containing month names (e.g., “December”) that does not appear in the context. Compared to a grounded token, the attention distribution associated with this hallucinated token exhibits noticeably stronger local fluctuations across context positions, with sharper peaks and more abrupt changes.

Therefore, we argue that directly mapping an attention sequence to a single scalar cannot fully capture the structure of attention patterns. Inspired by signal processing, we treat attention weights over context tokens as a discrete temporal signal indexed by token position, where stable grounding corresponds to smooth, slowly varying signals, while instability manifests as rapid local oscillations. To explicitly quantify such variation, we perform frequency-aware decomposition of the attention signal: low-frequency components capture global trends of attention allocation across the context, whereas high-frequency components isolate sharp spikes and abrupt local changes. We hypothesize that hallucinated tokens are associated with energy in these high-frequency attention components.

Motivated by this perspective, we study contextual hallucination detection via frequency-aware analysis of attention signals. Our contributions are threefold: (1) We formulate attention as discrete signals and introduce a unified frequency-based framework for analyzing attention variation for hallucination detection. (2) We instantiate this framework using simple yet efficient high-frequency extraction operators, enabling the quantification of attention instability at both token and span levels. (3) Through extensive experiments across multiple models and tasks, we show that frequency-based attention features can improve hallucination detection over existing verification-based, internal representation-based, and attention-based baselines.

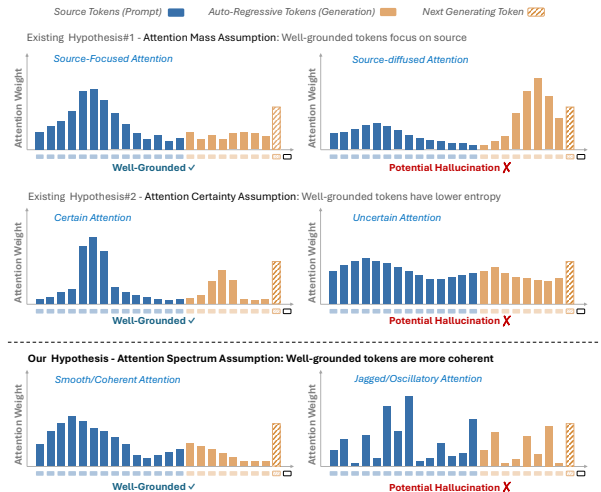


Figure 2. Three hypotheses for identifying hallucination tokens from incoming attention patterns. We illustrate three representative assumptions for distinguishing well-grounded tokens (✓) from potential hallucinations (✗) based on the incoming attention to the next generated token.

2. Background

In this section, we review attention weight as an intrinsic signal for hallucination and introduce a frequency-based perspective that characterizes attention instability beyond the coarse allocation statistics.

2.1. Attention-based Hallucination Detection

For each generated token, the attention distribution reflects how the model aggregates information from the source context and previously generated tokens, and is therefore widely used as an intrinsic signal of grounding and information usage (Campbell et al., 2023; Li et al., 2023; Snyder et al., 2024; Huang et al., 2025). Prior work exploits attention for hallucination detection by making different assumptions about grounded generation behavior.

One line of work focuses on attention transitions, using backward attention from generated tokens to the source context as an indicator of grounding (Chuang et al., 2024a; Ogasa & Arase, 2025). Another line analyzes the distributional properties of attention, either by identifying context tokens emphasized by specific attention heads (Sun et al., 2025) or by summarizing attention uncertainty using entropy-based measures (Vazhentsev et al., 2025). These approaches are motivated by the intuition that grounded generation exhibits focused and consistent evidence attribution, whereas hallucination is associated with diffuse or ambiguous attention.

As illustrated in Figure 2, existing attention-based methods primarily capture *where* attention is allocated or *how* dis-

persed it is, but do not explicitly model the internal structure of attention patterns. In contrast, our hypothesis emphasizes the *coherence* of attention distributions, motivated by the observation that hallucinated generations often exhibit fragmented or rapidly oscillating attention behavior that is not captured by static allocation or entropy-based statistics.

2.2. A Frequency-based View of Attention

To capture attention variation beyond static summaries, we model attention weights over tokens as discrete signals. In signal processing, smooth and coherent patterns are naturally represented by low-frequency components, whereas abrupt changes and local irregularities manifest as high-frequency components. As such, frequency analysis offers a natural characterization of attention stability and instability.

Rather than committing to a single formulation, we consider several standard operators that instantiate this frequency-based view with complementary inductive biases. The Discrete Fourier Transform (DFT) (Cooley et al., 1969) provides a global decomposition of attention signals into frequency components. The Discrete Wavelet Transform (DWT) (Mallat, 1989) uses localized basis functions, allowing abrupt attention changes to be captured while preserving positional information. As a simpler local alternative, the discrete Laplacian operator (Oppenheim & Schaffer, 1997) directly highlights second-order differences directly in the token domain, acting as an implicit high-pass filter.

Despite their different forms, these operators share a common goal: isolating high-frequency variation that reflects fragmented or rapidly oscillating attention behavior. Together, they provide a unified frequency-based framework for analyzing attention instability during generation.

3. Frequency-Aware Attention Modeling

Viewing attention from a frequency-aware perspective offers a principled way to analyze variation patterns that are difficult to characterize directly in the token domain. In this framework (shown in Figure 3), attention weights over tokens are modeled as discrete signals, enabling the use of frequency-aware operators to quantify how attention evolves and fluctuates during generation, beyond what is captured by aggregate statistics. We first demonstrate our motivation and intuition through a simplified setting here.

3.1. Motivation and Intuition

While a rigorous mechanistic understanding of attention behavior under hallucinated generation remains an open problem, we can gain preliminary insights from a simplified toy setting. Specifically, consider a scenario where tokens come from several latent semantic sources. As the number of such sources increases, neighboring tokens are more

likely to differ in topic, causing the compatibility between the current token and its context to change abruptly across adjacent positions. Such abrupt local changes translate into adjacent differences in attention weights, yielding jagged attention patterns along the sequence (see Appendix A for a complete proof). Although such toy analysis relies on simplifying assumptions, it formalizes a general link between semantic heterogeneity and attention instability.

Real LLM attention is, however, substantially far more complex. It is shaped by architectural depth, multi-head specialization, and long-range contextual interactions, all of which can give rise to higher-order and multi-scale instabilities that cannot be captured by adjacent difference measures alone. From a signal-processing perspective, adjacent differences correspond only to a primitive form of high-pass filtering. Frequency-aware operators (e.g., DFT, DWT, Laplacian), by contrast, are able to systematically extract high-frequency components across multiple resolutions (Donoho & Johnstone, 1998; Stein & Shakarchi, 2011). This motivates our frequency-aware framework for quantifying complex attention instabilities associated with hallucination detection.

3.2. Problem Setup

We consider a context-based generation setting, where a language model generates a response $\mathbf{gen} = (gen_1, \dots, gen_T)$ conditioned on a retrieved context $\mathbf{ctx} = (ctx_1, \dots, ctx_N)$. At each generation step i , the model produces token t_i based on $(\mathbf{ctx}, \mathbf{gen}_{<i})$ and exposes attention weights across layers and heads. Our primary task is token-level hallucination detection: for each generated token t_i , predict whether t_i is supported by the provided context.

Rather than operating on attention weights directly, our detector uses frequency-aware features derived from attention. For each step i when generating t_i , we compute a feature vector \mathbf{v} (defined in §3.4) and predict

$$\hat{r}_i = f(\mathbf{v}), \quad (1)$$

where $f(\cdot)$ is a lightweight linear classifier, and \hat{r}_i indicates a prediction result for hallucination or non-hallucination.

3.3. Attention as Discrete Signals

At generation step i , we extract attention weight distributions from all transformer layers and heads. We distinguish two types of attention signals: *context-directed attention*, attending from the current token t_i to the input context tokens, and *generated-token attention*, attending to previously generated tokens before this generation step.

For each layer $l \in \{1, \dots, L\}$ and head $h \in \{1, \dots, H\}$, we define the context-directed attention vector and the

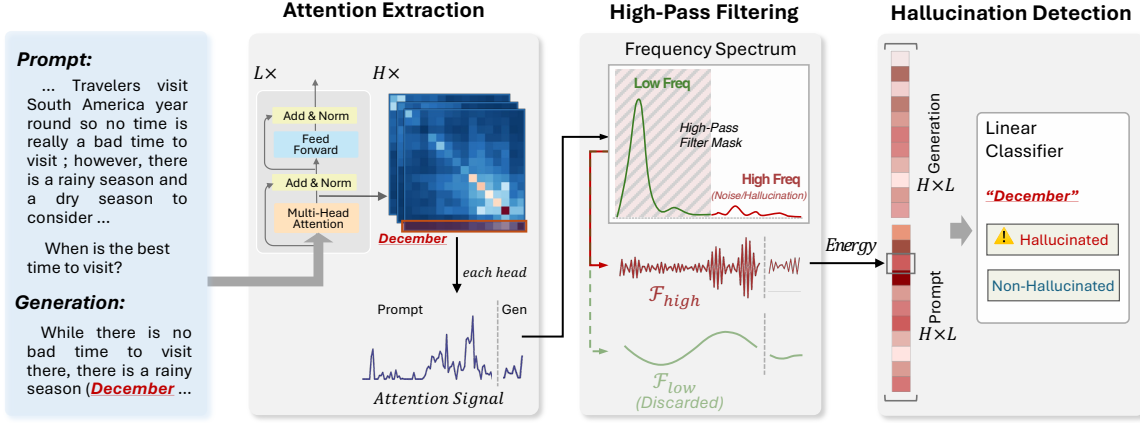


Figure 3. Overview of frequency-aware attention modeling for hallucination detection. Attention weights are extracted from each layer and head (L layers and H heads in total), treated as token-level signals, and decomposed using high-pass filtering to isolate high-frequency variations ($\mathcal{F}_{\text{high}}$), whose energy is aggregated for hallucination detection.

generated-token attention vector:

$$\begin{aligned} a_{l,h}^{(ctx)} &= [a_{l,h,1}^{(ctx)}, a_{l,h,2}^{(ctx)}, \dots, a_{l,h,N}^{(ctx)}] \in \mathbb{R}^N, \\ a_{l,h}^{(gen)} &= [a_{l,h,1}^{(gen)}, a_{l,h,2}^{(gen)}, \dots, a_{l,h,i-1}^{(gen)}] \in \mathbb{R}^{i-1}, \end{aligned} \quad (2)$$

which respectively capture attention over N context tokens and the previously generated tokens before t_i .

Both $a_{l,h}^{(ctx)}$ and $a_{l,h}^{(gen)}$ are treated as one-dimensional discrete signals that indexed by token position. Taking the Discrete Fourier Transform (DFT) as an example, and let $\mathcal{F}(\cdot)$ denote DFT. Mapping the attention weight vector to the frequency domain yields

$$\hat{a}_{l,h}^{(\tau)} = \mathcal{F}(a_{l,h}^{(\tau)}), \quad (3)$$

where $\tau \in \{ctx, gen\}$; details for the DWT and Laplacian operators are provided in Appendix B.

3.4. Energy-Based High-Frequency Instability

Building on the frequency-based view, we isolate and quantify high-frequency components of attention weight signals. The formulation applies uniformly to both context-directed and previously generated-token attention. To simplify notation, we use $\mathbf{x} \in \mathbb{R}^n$ to denote the attention signal obtained for t_i , corresponding to either $a_{l,h}^{(ctx)}$ or $a_{l,h}^{(gen)}$ for layer l and head h , with signal length n .

Given an attention signal \mathbf{x} , we extract high-frequency component by high-pass operator (e.g., DFT, DWT, Laplacian)

$$\mathbf{z}^{\text{hf}} = \mathcal{F}_{\text{high}}(\mathbf{x}), \quad (4)$$

where $\mathcal{F}_{\text{high}}$ denotes a high-pass operator that suppresses smooth, low-frequency components while preserving high-frequency components representing rapid local variation.

For transform-based operators such as DFT and DWT, $\mathcal{F}_{\text{high}}$ is implemented by frequency-domain masking followed by an inverse transform. Let $\hat{\mathbf{x}} = \mathcal{F}(\mathbf{x})$ denote the DFT coefficients. We retain only high-frequency components by applying a frequency mask by following definition:

$$\hat{\mathbf{x}}_k^{\text{hf}} = \begin{cases} \hat{\mathbf{x}}_k, & k \in \mathcal{K}_{\text{high}}, \\ 0, & \text{otherwise,} \end{cases} \quad (5)$$

where $\mathcal{K}_{\text{high}}$ indexes the retained high-frequency band. The corresponding high-frequency component \mathbf{z}^{hf} in the temporal domain is obtained via inverse transform. Wavelet- and Laplacian-based operators provide alternative realizations of $\mathcal{F}_{\text{high}}$ that emphasize localized high-frequency variation, while serving the same purpose of isolating rapid attention fluctuations (detailed in Appendix B).

We summarize the magnitude of high-frequency variation by using the ℓ_2 norm on the high-frequency component

$$\rho = \|\mathbf{z}^{\text{hf}}\|_2, \quad (6)$$

which measures the energy of high-frequency components in the attention signal in temporal domain.

The use of the ℓ_2 norm is theoretically motivated by **Parseval's theorem**, which establishes the equivalence between signal energy measured in the temporal domain and that measured in the frequency domain. For DFT-based filtering,

$$\|\mathbf{z}^{\text{hf}}\|_2^2 = \sum_{j=1}^n |\mathbf{z}_j^{\text{hf}}|^2 = \frac{1}{n} \sum_{k=0}^{n-1} |\hat{\mathbf{x}}_k^{\text{hf}}|^2. \quad (7)$$

Applying the above procedure independently to each attention head and each attention type yields a score $\rho_{l,h}^{(\tau)}$ for

Table 1. Comparison of different methods on RAGTruth and HalluRAG. Wavelet-high and Fourier-high denote leveraging the high-frequency components obtained via DWT and DFT, respectively. **Bold** and underlined values indicate the best and second-best performance within each model group.

Model	Method	RT-QA		RT-D2T		RT-Summ		HalluRAG		Overall Avg.	
		F	AUROC	F	AUROC	F	AUROC	F	AUROC	Avg-F	Avg-A
LLaMA-7B	SelfcheckGPT	0.6289	0.6942	0.6552	0.8026	0.6349	0.6674	0.5388	0.5963	0.6145	0.6901
	RefChecker	0.5914	0.5865	0.5713	0.6349	<u>0.6059</u>	0.6080	0.5819	0.5722	0.5876	0.6004
	EigenScore	0.4979	0.5253	0.5256	0.5297	0.5065	0.4989	0.5364	0.6127	0.5166	0.5416
	Redeep	0.5972	0.6364	0.4791	0.3960	0.5897	0.5760	0.5912	0.6490	0.5643	0.5643
	Lookback-lens	0.6930	0.8482	0.6175	0.8442	0.5328	0.7156	0.6266	0.7405	0.6175	0.7871
	Attn-variance	0.4807	0.6147	0.4839	0.5890	0.4886	0.6492	0.4489	0.5571	0.4755	0.6025
	Attn-entropy	0.6832	0.8481	0.6011	0.8368	0.5031	0.6722	0.6020	0.6937	0.5973	0.7627
	Laplacian	0.7107	0.8449	<u>0.6878</u>	0.8519	0.5779	0.7040	0.6370	0.7429	0.6534	0.7859
	Wavelet-high	0.7194	<u>0.8526</u>	0.6898	0.8569	0.5929	<u>0.7165</u>	0.6384	<u>0.7550</u>	<u>0.6601</u>	0.7953
Fourier-high	0.7277	0.8584	0.6870	0.8595	0.5875	0.7426	0.6438	0.7603	0.6615	0.8052	
LLaMA-13B	SelfcheckGPT	0.6029	0.6425	0.6346	0.7989	0.5554	0.5909	0.6337	0.7216	0.6066	0.6885
	RefChecker	0.5928	0.5893	0.5784	0.6381	<u>0.5924</u>	0.6346	0.6098	0.5963	0.5934	0.6146
	EigenScore	0.4788	0.4734	0.6063	0.6582	0.5121	0.5097	0.6316	0.6947	0.5572	0.5840
	Redeep	0.5740	0.6457	0.5273	0.6449	0.5010	0.5253	0.5769	0.6294	0.5448	0.6113
	Lookback-lens	0.6947	0.8727	0.7137	0.8766	0.5679	0.6702	0.6594	0.7929	0.6589	0.8031
	Attn-variance	0.5636	0.7497	0.5992	0.7177	0.4947	0.6629	0.4529	0.6298	0.5276	0.6900
	Attn-entropy	0.6909	0.8650	0.7034	0.8717	0.5527	0.6865	0.6284	0.7270	0.6438	0.7875
	Laplacian	0.6834	0.8552	0.7194	0.8796	0.5548	0.6700	<u>0.6659</u>	0.7624	0.6559	0.7918
	Wavelet-high	0.7029	<u>0.8741</u>	0.7383	0.8932	0.5651	0.7042	0.6684	0.7809	0.6687	0.8131
Fourier-high	0.7068	0.8792	<u>0.7278</u>	<u>0.8825</u>	0.5929	0.7362	0.6616	<u>0.7899</u>	0.6723	0.8198	
Mistral-7B	SelfcheckGPT	0.6551	0.7084	0.6958	0.8353	0.6966	0.7166	0.5515	0.6473	0.6498	0.7269
	RefChecker	0.6144	0.6121	0.5907	0.6287	0.6664	0.6596	0.6176	0.6031	0.6223	0.6259
	EigenScore	0.4904	0.4611	0.5449	0.6507	0.4582	0.4973	0.6581	0.7924	0.5379	0.6004
	Redeep	0.6270	0.7357	0.6013	0.6648	0.5379	0.5680	0.4987	0.5646	0.5662	0.6333
	Lookback-lens	0.7832	0.9148	0.7151	0.8845	0.6759	0.7954	0.7115	0.7966	0.7214	0.8478
	Attn-variance	0.5636	0.7497	0.6218	0.7021	0.4840	0.5836	0.5367	0.6953	0.5515	0.6827
	Attn-entropy	0.7810	0.9083	0.7049	0.8734	0.6551	0.7867	0.6803	0.7504	0.7053	0.8297
	Laplacian	0.7807	0.9049	<u>0.7255</u>	<u>0.8849</u>	0.6723	0.7978	0.7001	0.8098	0.7197	0.8494
	Wavelet-high	0.7876	0.9117	0.7136	0.8829	0.6849	0.8075	0.7274	0.8360	0.7284	0.8595
Fourier-high	0.7885	0.9099	0.7267	0.8863	0.6761	<u>0.8037</u>	<u>0.7152</u>	0.8128	<u>0.7266</u>	<u>0.8532</u>	

every layer l , head h , and attention type $\tau \in \{ctx, gen\}$.

$$\begin{aligned} \mathbf{v}^{(\tau)} &= [\rho_{1,1}^{(\tau)}, \rho_{1,2}^{(\tau)}, \dots, \rho_{L,H}^{(\tau)}]^\top, \quad \tau \in \{ctx, gen\}, \\ \mathbf{v} &= [\mathbf{v}^{(ctx)}; \mathbf{v}^{(gen)}]. \end{aligned} \quad (8)$$

We aggregate these scores across all layers and heads to form feature vectors $\mathbf{v}^{(ctx)}$ and $\mathbf{v}^{(gen)}$ for context-directed and generated-token attention, respectively. We then concatenate these vectors as \mathbf{v} and feed them into the classifier to obtain the final prediction \hat{r}_i for token-level hallucination detection. As a robustness check under coarser supervision, we also report span-level results by applying a fixed sliding window, averaging the feature vectors within each window, and feeding the averaged vectors into the classifier.

4. Experiment Setting

4.1. Baselines

In this study, we evaluate our approach against a diverse set of representative baselines for comparison, span-

ning verification-based, internal representation-based, and attention-based paradigms, as detailed below.

Verification-based Methods. **SelfCheckGPT** (Manakul et al., 2023) detects hallucinations by measuring stochastic consistency across multiple responses sampled from a language model. **RefChecker** (Hu et al., 2024b) extracts claims from model outputs and verifies them against context using a dedicated checker. Both of them operate in a prompt-based manner and rely on the generative behavior of the underlying LLM.

Internal Representation-Based Methods. **EigenScore** (Chen et al., 2024) leverages output probability distributions to construct a semantic consistency graph and quantifies uncertainty via spectral analysis. **ReDeEP** integrates internal signals from hidden states and attention mass to detect hallucinations (Sun et al., 2025). Both methods represent strong internal-signal-based baselines.

Attention-based Methods. We include **Lookback-Lens**

(Chuang et al., 2024a) as a strong attention-based baseline, which characterizes hallucination by quantifying the allocation of attention between retrieved context tokens and previously generated tokens. In addition, we implement two mechanistic attention-based baselines based on attention **variance** and attention **entropy**. For these baselines, statistics are computed separately over context tokens and generated tokens, and concatenated across all attention heads to form a unified feature representation for classification.

4.2. Implementation Settings

To evaluate the effectiveness and robustness of our method, we conduct experiments across three widely used open-source LLMs, including LLaMA-7B-Chat, LLaMA-13B-Chat, and Mistral-7B-Instruct, covering diverse model sizes and architectures. Experiments are conducted on two context-based hallucination benchmarks: RAGTruth (Niu et al., 2024), covering question answering (QA), data-to-text (D2T), and summarization (Summ), and HalluRAG (Ridder & Schilling, 2024), which focuses on the QA task. Both datasets provide token-level hallucination annotations. Frequency-aware attention features are aggregated using a single-layer logistic regression classifier, and detection is performed at either the token or span level. We report F1 and AUROC on the test sets, using AUROC as the primary metric. Additional details are provided in Appendix C.3.

5. Results and Analysis

5.1. Overall Performance

Across all evaluated models and datasets, frequency-aware analysis of attention consistently improves hallucination detection over verification-based, internal representation-based, and attention-based baselines. Explicitly isolating high-frequency components of attention yields stronger performance than aggregate statistics such as variance or entropy, highlighting the importance of modeling fine-grained attention variation. By focusing on *how* attention varies within the sequence rather than *where* attention mass is allocated, frequency-aware features provide complementary discriminative signals beyond attention mass alone.

These improvements hold across diverse task formats and models. For example, on summarization task, Fourier-high improves AUROC by 6.6% over Lookback-Lens on LLaMA-13B, and by 2.7% on LLaMA-7B. This consistency across datasets and generation settings suggests that high-frequency attention variation captures a general property of ungrounded generation, rather than task- or structure-specific artifacts. We further evaluate cross-domain generalization by training the detector on one task and testing it on another (see Table A2). Compared to Lookback-Lens, our method exhibits substantially more robust transfer perfor-

mance, indicating that frequency-aware attention features generalize better across task boundaries.

Among all three operators, Fourier-based features achieve the strongest overall performance, followed by wavelets and the Laplacian. This ordering aligns with both their inductive biases and the structural properties of attention signals: attention distributions are typically sparse and highly uneven across positions (Nawrot et al., 2025), often dominated by a small subset of tokens, which favors operators that aggregate high-frequency variation globally. Correspondingly, Fourier-based filtering is particularly effective at capturing global high-frequency energy, while wavelets and the Laplacian emphasize progressively more localized variation.

Table 2. Performance comparison on RagTruth-Avg and HalluRAG for sliding-window=8. Within each model, the best result is highlighted in **bold**, and the second-best is underlined.

Model	Method	RagTruth-Avg		HalluRAG	
		F	AUROC	F	AUROC
LLaMA-7B	Lookback-lens	0.6773	0.7884	0.6623	0.7856
	Laplacian	0.6747	0.7877	0.6775	0.7754
	Wavelet-High	0.6911	0.8117	0.6812	0.7928
	Fourier-high	0.7003	0.8412	0.6866	0.8100
LLaMA-13B	Lookback-lens	0.6781	0.8183	0.7096	0.8505
	Laplacian	0.6819	0.8039	0.7217	0.8264
	Wavelet-High	0.6953	0.8448	0.7417	0.8438
	Fourier-high	0.7063	0.8585	0.7217	0.8515
Mistral-7B	Lookback-lens	0.7554	0.8764	0.7752	0.8403
	Laplacian	0.7322	0.8495	0.8056	0.8920
	Wavelet-High	0.7597	0.8742	0.7682	0.8802
	Fourier-high	0.7663	0.8812	0.7883	0.8872

5.2. Span-level Hallucination Detection

In practical settings, hallucinations often occur as contiguous spans rather than isolated tokens. To evaluate whether our method generalizes beyond token-level detection, we conduct span-level hallucination detection under a sliding-window setting, where consecutive tokens are grouped into fixed-size chunks and classified at the chunk level. Following prior work such as Lookback-Lens, we use a chunk size of 8 and aggregate attention features within each chunk to form a single representation for prediction. Results across the two benchmarks are reported in Table 2, with full per-task results provided in Table A3 for RagTruth.

Span-level evaluation is more challenging due to coarser supervision and the need to aggregate signals across multiple tokens. Despite this increased difficulty, Fourier- and Wavelet-based variants achieve the strongest performance on all three tasks. Fourier-based features yield consistent gains over Lookback-Lens, improving AUROC by 5.3% on LLaMA-7B (RAGTruth-Avg), with a particularly improvement of 10.1% on the summarization task (see Table A3). Overall, these results indicate that frequency-based features remain robust when individual token-level signals are aggregated into spans, and that our approach generalizes naturally

from token- to span-level hallucination detection across multiple tasks without requiring architectural modification.

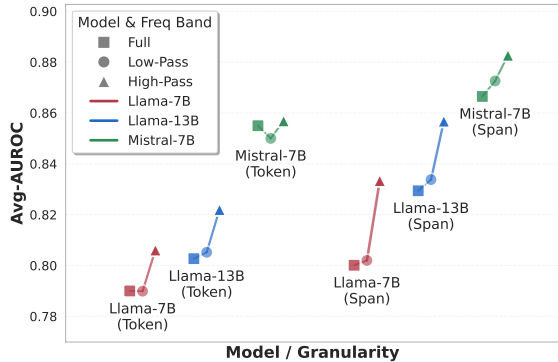


Figure 4. Comparing full-, low-, and high-pass Fourier attention features. Average AUROC across models under token- and span-level evaluation settings.

5.3. Ablation Study on High/Low-pass Components

We further analyze the contribution of different frequency bands by comparing low-pass, high-pass, and full-spectrum attention features, as shown in Figure 4. Across all models and both token- and span-level evaluation settings, high-pass components achieve the strongest performance, while low-pass and full-spectrum features perform comparably. This pattern suggests that, without explicitly isolating high-frequency variation, attention signals are largely dominated by low-frequency components that offer limited discriminative power for hallucination detection.

Low-frequency components mainly reflect smooth, global alignment patterns common to both grounded and hallucinated outputs, whereas high-pass components emphasize rapid local irregularities in attention that are more closely associated with unstable generation behavior. Additional analyses on Fourier frequency cutoffs and Wavelet detail levels are provided in Figure A1, Table A4, and Table A5.

5.4. Understanding Frequency-Aware Features

To better understand how frequency-aware attention features contribute to hallucination detection, we analyze the learned linear classifier from three perspectives: layer-level importance, head-level sparsity, and the relative contribution of context versus generated attention.

5.4.1. LAYER-WISE IMPORTANCE

As shown in Figure 5, we report the average absolute classifier coefficients assigned to attention heads in each layer. The importance of high-frequency attention signals is clearly non-uniform across model depth. For Fourier-based features, importance peaks in the middle layers, with a pronounced maximum around layer 14. These layers are com-

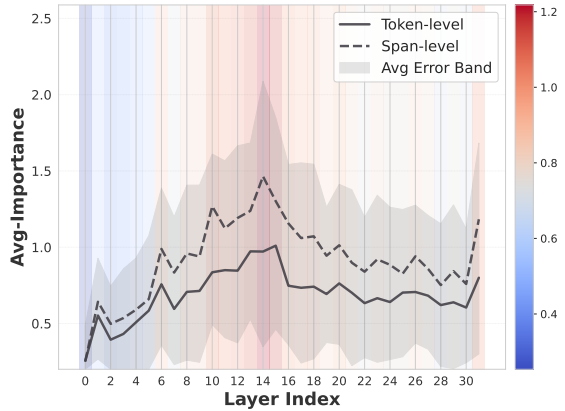


Figure 5. Layer-wise importance of high-frequency Fourier-high attention features for LLaMA-7B.

monly associated with higher-level semantic processing and factual reasoning, suggesting that hallucination-related attention instability emerges most prominently once the model gradually transitions from surface-level decoding to semantic composition (Chuang et al., 2024b).

Across almost all layers, span-level (dashed line) assigns higher importance weights than token-level detection (solid line). This indicates that aggregating attention signals over longer spans amplifies structured high-frequency variation, rather than weakening it, further supporting the robustness of frequency-aware features under coarser supervision.

5.4.2. HEAD-WISE SPARSITY

Beyond layer-level trends, we examine whether detection signals are broadly distributed across heads or concentrated in a small subset. To this end, we perform detection using only the Top- k attention heads ranked by their average absolute classifier coefficients.

Table 3. AUROC Results for LLaMA-7B: Original vs. Top- k head only performance.

RagTruth-Avg				
Method	Original	Top- k heads		
		$k = 100$	50	10
Laplacian	0.8003	0.7824	0.7666	0.7131
Wavelet-high	0.8087	0.7900	0.7708	0.7193
Fourier-high	0.8205	0.7915	0.7684	0.6995
HalluRAG				
Method	Original	Top- k heads		
		$k = 100$	50	10
Laplacian	0.7429	0.7222	0.6986	0.6479
Wavelet-high	0.7550	0.7229	0.7016	0.6562
Fourier-high	0.7629	0.7229	0.6814	0.6373

As shown in Table 3, a remarkably small fraction of heads

accounts for most of the detection performance. Using only the top 100 heads (less than 10% of all heads in LLaMA-7B) recovers over 95% of the original AUROC across operators and datasets. This pronounced sparsity indicates that hallucination-related high-frequency attention variation is not a diffuse property shared across all heads. Instead, a small subset of heads consistently exhibits strong sensitivity to attention instability, suggesting that these heads act as implicit internal indicators of ungrounded generation.

5.4.3. CONTEXT V.S. GENERATED ATTENTION CONTRIBUTION

A critical design choice in our method is incorporating high-frequency attention signals from both source context tokens and previously generated tokens during generation. We analyze the learned classifier to assess the relative importance of these two sources in practice.

As shown in Figure 6, frequency-aware signals derived from context-token attention are consistently more informative for hallucination detection than those from generated-token attention across all spectral operators. Among them, the Fourier-based method exhibits the largest context-generated importance gap, which aligns with its superior overall performance across tasks and models, suggesting that capturing frequency-aware patterns in context attention contributes to more robust hallucination detection.

This asymmetry aligns closely with the core motivation of Lookback-lens (Chuang et al., 2024a), which emphasizes the role of backward attention to contextual evidence in grounded generation. Our results extend this view by showing that not only the presence of backward attention, but also its stability and variation, play a critical role in practice. This interpretation is further supported by more ablation results in Table A7, where removing only context-based features leads to substantially larger performance degradation than removing only generated-token features.

6. Broader Related Work

In this section, we briefly situate our work within the broader literature on hallucination detection in LLMs.

A substantial line of work detects hallucinations through **external knowledge verification**, validating model outputs against curated corpora, knowledge bases, or web search results (Min et al., 2023; Feng et al., 2023b; Chern et al., 2023). While effective when reliable evidence is available, these approaches are constrained by knowledge coverage, retrieval quality, and inference-time latency, limiting their applicability in on-the-fly detection settings.

In contrast, **intrinsic detection** methods rely solely on model-internal signals and are lightweight enough to op-

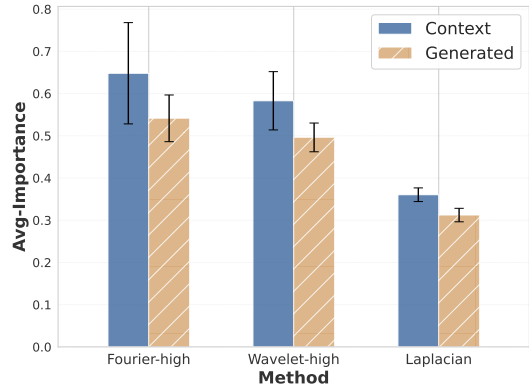


Figure 6. Average absolute classifier importance assigned to context-attention and generated-attention features over all examined models and datasets.

erate during decoding. Prior work has explored semantic consistency between input and output, uncertainty and self-consistency across generations, and generation-time statistics such as token probabilities or hidden-state geometry (Qi et al., 2025). More recent studies probe attention mechanisms as intrinsic indicators of hallucination (Sun et al., 2025; Chuang et al., 2024a; Campbell et al., 2023), which mainly characterize where attention is allocated or how concentrated it is, but largely overlook fine-grained local variation within the token sequence.

Using **frequency-aware** tools offers an additional perspective for examining internal model dynamics (Kiruluta, 2025; Li et al., 2025). By modeling internal signals as discrete sequences, frequency-aware representations capture structural patterns that are difficult to characterize using token-level statistics alone. Attention distributions are also typically sparse and highly non-uniform across token positions (Nawrot et al., 2025; Gu et al., 2025), providing a natural basis for frequency-based decomposition, where abrupt allocation correspond to high-frequency components and global distribution patterns align with low-frequency trends.

Building on this perspective, our work introduces a frequency-aware characterization of attention variation as an intrinsic signal for hallucination detection.

7. Conclusion

This work presents a frequency-aware perspective for analyzing hallucination in LLMs. We show that hallucinated generation is associated with high-frequency variation in attention patterns, revealing a structural property of model behavior that is not captured by attention allocation, transition, or aggregate uncertainty measures. This provides a principled way to distinguish grounded from ungrounded generation based on how attention varies across tokens.

Building on this insight, we introduce a frequency-aware

attention modeling framework that extracts high-frequency attention signals using spectral operators. Across multiple models and tasks, our approach improves hallucination detection at both token and span levels, indicating its potential as a generalizable and task-agnostic intrinsic signal for analysis. Overall, our findings suggest that hallucinations are reflected not only in where attention is placed, but also in how it varies across tokens over time, highlighting frequency-aware analysis as a promising direction for diagnosing and mitigating unreliable LLM generation.

Acknowledgements

SQ is funded by a PhD scholarship provided by K-CSC. YH was supported by the UK Engineering and Physical Sciences Research Council (EPSRC) through a Turing AI Fellowship (grant no. EP/V020579/1, EP/V020579/2). The authors acknowledge the use of King’s Computational Research, Engineering and Technology Environment (CREATE) at King’s College London.

Impact Statement

This paper presents a frequency-aware analysis of internal attention in LLMs for detecting hallucinated generation. The goal of this work is to advance the understanding and evaluation of LLMs by providing intrinsic signals that can help identify unreliable outputs.

There are potential positive societal impacts of this work, including improved reliability and transparency of language model deployments in applications where factual correctness is important. By relying solely on model-internal signals, the proposed approach avoids dependence on external knowledge sources and may be used as a lightweight evaluation tool.

At the same time, this work does not aim to prevent hallucination or provide guarantees of correctness, and the signals identified should not be used as the sole basis for high-stakes decisions. As with other analysis and detection methods, responsible deployment requires appropriate safeguards and complementary evaluation mechanisms. Overall, we believe the ethical and societal implications of this work are aligned with well-established goals in machine learning research, and do not warrant further specific discussion.

References

Campbell, J., Ren, R., and Guo, P. Localizing Lying in Llama: Understanding Instructed Dishonesty on True-false Questions Through Prompting, Probing, and Patching. *CoRR*, abs/2311.15131, 2023. doi: 10.48550/ARXIV.2311.15131. URL <https://doi.org/10.48550/arXiv.2311.15131>.

Chen, C., Liu, K., Chen, Z., Gu, Y., Wu, Y., Tao, M., Fu, Z., and Ye, J. INSIDE: LLMs’ Internal States Retain the Power of Hallucination Detection. In *The Twelfth International Conference on Learning Representations, ICLR 2024, Vienna, Austria, May 7-11, 2024*. OpenReview.net, 2024. URL <https://openreview.net/forum?id=Zj12nzlQbz>.

Chern, I., Chern, S., Chen, S., Yuan, W., Feng, K., Zhou, C., He, J., Neubig, G., and Liu, P. FacTool: Factuality Detection in Generative AI - A Tool Augmented Framework for Multi-task and Multi-domain Scenarios. *CoRR*, 2023. doi: 10.48550/ARXIV.2307.13528.

Chuang, Y., Qiu, L., Hsieh, C., Krishna, R., Kim, Y., and Glass, J. R. Lookback Lens: Detecting and Mitigating Contextual Hallucinations in Large Language Models Using Only Attention Maps. In *EMNLP*, pp. 1419–1436, 2024a.

Chuang, Y., Xie, Y., Luo, H., Kim, Y., Glass, J. R., and He, P. DoLa: Decoding by Contrasting Layers Improves Factuality in Large Language Models. In *The Twelfth International Conference on Learning Representations, ICLR 2024, Vienna, Austria, May 7-11, 2024*. OpenReview.net, 2024b. URL <https://openreview.net/forum?id=Th6NyL07na>.

Cooley, J. W., Lewis, P. A. W., and Welch, P. D. The Fast Fourier Transform and Its Applications. *IEEE Transactions on Education*, 12(1):27–34, 1969. doi: 10.1109/TE.1969.4320436.

Donoho, D. L. and Johnstone, I. M. Minimax estimation via wavelet shrinkage. *The annals of Statistics*, 26(3): 879–921, 1998.

Feng, J., Yang, L., Li, Z., Zhang, J., et al. Trustworthy LLMs: A Survey and Guideline for Evaluating Large Language Models’ Alignment. *arXiv preprint arXiv:2308.05374*, 2023a.

Feng, S., Balachandran, V., Bai, Y., and Tsvetkov, Y. FactKB: Generalizable Factuality Evaluation using Language Models Enhanced with Factual Knowledge. In Bouamor, H., Pino, J., and Bali, K. (eds.), *Proceedings of the 2023 Conference on Empirical Methods in Natural Language Processing*, pp. 933–952, Singapore, 2023b. Association for Computational Linguistics. doi: 10.18653/v1/2023.emnlp-main.59. URL <https://aclanthology.org/2023.emnlp-main.59>.

Gong, X., Ming, T., Wang, X., and Wei, Z. DAMRO: Dive into the Attention Mechanism of LVLm to Reduce Object Hallucination. In Al-Onaizan, Y., Bansal, M., and Chen, Y. (eds.), *Proceedings of the 2024 Conference on Empirical Methods in Natural Language*

- Processing, *EMNLP 2024, Miami, FL, USA, November 12-16, 2024*, pp. 7696–7712. Association for Computational Linguistics, 2024. doi: 10.18653/V1/2024.EMNLP-MAIN.439. URL <https://doi.org/10.18653/v1/2024.emnlp-main.439>.
- Gu, X., Pang, T., Du, C., Liu, Q., Zhang, F., Du, C., Wang, Y., and Lin, M. When Attention Sink Emerges in Language Models: An Empirical View. In *The Thirteenth International Conference on Learning Representations, ICLR 2025, Singapore, April 24-28, 2025*. OpenReview.net, 2025. URL <https://openreview.net/forum?id=78Nn4QJTEN>.
- Hu, H., Sun, Y., and Zhang, Q. LRP4RAG: Detecting Hallucinations in Retrieval-augmented Generation via Layer-wise Relevance Propagation. *CoRR*, 2024a. doi: 10.48550/ARXIV.2408.15533.
- Hu, X., Ru, D., Qiu, L., Guo, Q., Zhang, T., Xu, Y., Luo, Y., Liu, P., Zhang, Y., and Zhang, Z. RefChecker: Reference-based Fine-grained Hallucination Checker and Benchmark for Large Language Models. *CoRR*, abs/2405.14486, 2024b. doi: 10.48550/ARXIV.2405.14486. URL <https://doi.org/10.48550/arXiv.2405.14486>.
- Huang, Y., Zhang, Y., Cheng, N., Li, Z., Wang, S., and Xiao, J. Dynamic Attention-guided Context Decoding for Mitigating Context Faithfulness Hallucinations in Large Language Models. *CoRR*, abs/2501.01059, 2025. doi: 10.48550/ARXIV.2501.01059. URL <https://doi.org/10.48550/arXiv.2501.01059>.
- Ji, Z., Lee, N., Frieske, R., Yu, T., Su, D., Xu, Y., Ishii, E., Bang, Y., Madotto, A., and Fung, P. Survey of Hallucination in Natural Language Generation. *ACM Comput. Surv.*, pp. 248:1–248:38, 2023. doi: 10.1145/3571730.
- Kiruluta, A. From Attention to Atoms: Spectral Dictionary Learning for Fast, Interpretable Language Models. *CoRR*, abs/2505.00033, 2025. doi: 10.48550/ARXIV.2505.00033. URL <https://doi.org/10.48550/arXiv.2505.00033>.
- Kryscinski, W., McCann, B., Xiong, C., and Socher, R. Evaluating the Factual Consistency of Abstractive Text Summarization. In Webber, B., Cohn, T., He, Y., and Liu, Y. (eds.), *Proceedings of the 2020 Conference on Empirical Methods in Natural Language Processing, EMNLP 2020, Online, November 16-20, 2020*, pp. 9332–9346. Association for Computational Linguistics, 2020. doi: 10.18653/V1/2020.EMNLP-MAIN.750. URL <https://doi.org/10.18653/v1/2020.emnlp-main.750>.
- Laban, P., Schnabel, T., Bennett, P. N., and Hearst, M. A. SummaC: Re-visiting NLI-based Models for Inconsistency Detection in Summarization. *Trans. Assoc. Comput. Linguistics*, 10:163–177, 2022. doi: 10.1162/TACL_A_00453. URL https://doi.org/10.1162/tacl_a_00453.
- Li, J., Tu, G., Cheng, S., Hu, J., Wang, J., Chen, R., Zhou, Z., and Shan, D. LLM Hallucination Detection: A Fast Fourier Transform Method Based on Hidden Layer Temporal Signals. *CoRR*, abs/2509.13154, 2025. doi: 10.48550/ARXIV.2509.13154. URL <https://doi.org/10.48550/arXiv.2509.13154>.
- Li, K., Patel, O., Viégas, F. B., Pfister, H., and Wattenberg, M. Inference-time Intervention: Eliciting Truthful Answers from a Language Model. In Oh, A., Naumann, T., Globerson, A., Saenko, K., Hardt, M., and Levine, S. (eds.), *Advances in Neural Information Processing Systems 36: Annual Conference on Neural Information Processing Systems 2023, NeurIPS 2023, New Orleans, LA, USA, December 10 - 16, 2023*, 2023.
- Mallat, S. A theory for multiresolution signal decomposition: the wavelet representation. *IEEE Transactions on Pattern Analysis and Machine Intelligence*, 11(7):674–693, 1989. doi: 10.1109/34.192463.
- Manakul, P., Liusie, A., and Gales, M. SelfCheckGPT: Zero-resource Black-box Hallucination Detection for Generative Large Language Models. In Bouamor, H., Pino, J., and Bali, K. (eds.), *Proceedings of the 2023 Conference on Empirical Methods in Natural Language Processing*, pp. 9004–9017, Singapore, 2023. Association for Computational Linguistics. doi: 10.18653/v1/2023.emnlp-main.557. URL <https://aclanthology.org/2023.emnlp-main.557>.
- Min, S., Krishna, K., Lyu, X., Lewis, M., Yih, W.-t., Koh, P., Iyyer, M., Zettlemoyer, L., and Hajishirzi, H. FActScore: Fine-grained Atomic Evaluation of Factual Precision in Long Form Text Generation. In Bouamor, H., Pino, J., and Bali, K. (eds.), *Proceedings of the 2023 Conference on Empirical Methods in Natural Language Processing*, pp. 12076–12100, Singapore, 2023. Association for Computational Linguistics. doi: 10.18653/v1/2023.emnlp-main.741. URL <https://aclanthology.org/2023.emnlp-main.741>.
- Nawrot, P., Li, R., Huang, R., Ruder, S., Marchisio, K., and Ponti, E. M. The Sparse Frontier: Sparse Attention Trade-offs in Transformer LLMs. *CoRR*, abs/2504.17768, 2025. doi: 10.48550/ARXIV.2504.17768. URL <https://doi.org/10.48550/arXiv.2504.17768>.
- Niu, C., Wu, Y., Zhu, J., Xu, S., Shum, K., Zhong, R., Song, J., and Zhang, T. RAGTruth: A Hallucination Corpus for Developing Trustworthy Retrieval-augmented Language Models. In *ACL*, pp. 10862–10878, 2024. doi: 10.18653/v1/2024.acl-long.585.

- Ogasa, Y. and Arase, Y. Hallucinated Span Detection with Multi-view Attention Features. In *Proceedings of the 14th Joint Conference on Lexical and Computational Semantics (*SEM 2025)*, pp. 381–394, 2025.
- Oppenheim, A. V. and Schaffer, A. S. *Signals and Systems*. Prentice Hall, 2 edition, 1997.
- Qi, S., Gui, L., He, Y., and Yuan, Z. A Survey of Automatic Hallucination Evaluation on Natural Language Generation, 2025. URL <https://arxiv.org/abs/2404.12041>.
- Ridder, F. and Schilling, M. The HalluRAG Dataset: Detecting Closed-domain Hallucinations in RAG Applications Using an LLM’s Internal States. *CoRR*, abs/2412.17056, 2024. doi: 10.48550/ARXIV.2412.17056. URL <https://doi.org/10.48550/arXiv.2412.17056>.
- Sandryhaila, A. and Moura, J. M. F. Discrete Signal Processing on Graphs: Frequency Analysis. *IEEE Trans. Signal Process.*, 62(12):3042–3054, 2014. doi: 10.1109/TSP.2014.2321121. URL <https://doi.org/10.1109/TSP.2014.2321121>.
- Snyder, B., Moisesescu, M., and Zafar, M. B. On Early Detection of Hallucinations in Factual Question Answering. In Baeza-Yates, R. and Bonchi, F. (eds.), *Proceedings of the 30th ACM SIGKDD Conference on Knowledge Discovery and Data Mining, KDD 2024, Barcelona, Spain, August 25-29, 2024*, pp. 2721–2732. ACM, 2024. doi: 10.1145/3637528.3671796. URL <https://doi.org/10.1145/3637528.3671796>.
- Sriramanan, G., Bharti, S., Sadasivan, V. S., Saha, S., Kattakinda, P., and Feizi, S. LLM-Check: Investigating Detection of Hallucinations in Large Language Models. In Globersons, A., Mackey, L., Belgrave, D., Fan, A., Paquet, U., Tomczak, J. M., and Zhang, C. (eds.), *Advances in Neural Information Processing Systems 38: Annual Conference on Neural Information Processing Systems 2024, NeurIPS 2024, Vancouver, BC, Canada, December 10 - 15, 2024*, 2024.
- Stein, E. M. and Shakarchi, R. *Fourier analysis: an introduction*, volume 1. Princeton University Press, 2011.
- Sun, Z., Zang, X., Zheng, K., Xu, J., Zhang, X., Yu, W., Song, Y., and Li, H. ReDeEP: Detecting Hallucination in Retrieval-augmented Generation via Mechanistic Interpretability. In *ICLR*, 2025.
- van Deemter, K. The Pitfalls of Defining Hallucination. *Comput. Linguistics*, 50(2):807–816, 2024. doi: 10.1162/COLI_A_00509. URL https://doi.org/10.1162/coli_a_00509.
- Vazhentsev, A., Rvanova, L., Kuzmin, G., Fadeeva, E., Lazichny, I., Panchenko, A., Panov, M., Baldwin, T., Sachan, M., Nakov, P., and Shelmanov, A. Uncertainty-aware Attention Heads: Efficient Unsupervised Uncertainty Quantification for LLMs. *CoRR*, abs/2505.20045, 2025. doi: 10.48550/ARXIV.2505.20045. URL <https://doi.org/10.48550/arXiv.2505.20045>.
- Wiegreffe, S. and Pinter, Y. Attention is not not Explanation. In Inui, K., Jiang, J., Ng, V., and Wan, X. (eds.), *Proceedings of the 2019 Conference on Empirical Methods in Natural Language Processing and the 9th International Joint Conference on Natural Language Processing, EMNLP-IJCNLP 2019, Hong Kong, China, November 3-7, 2019*, pp. 11–20. Association for Computational Linguistics, 2019. doi: 10.18653/V1/D19-1002. URL <https://doi.org/10.18653/v1/D19-1002>.

A. A three-step proof that larger K increases (a lower bound on) attention roughness

Goal. We consider a *single-layer* causal self-attention mechanism and measure, at a fixed prediction position $t \geq 2$, how *rough* the attention weights over past positions are as a function of the number of mixture components K in the input distribution. Roughness is quantified by the ℓ_2 adjacent-difference energy

$$R_t \triangleq \sum_{j=1}^{t-2} (\alpha_{t,j+1} - \alpha_{t,j})^2, \quad (9)$$

where $\alpha_{t,1:t-1}$ is the attention row (probability vector) used to predict token t .

We prove the claim via three sub-claims: (i) adjacent tokens switch mixture components more often when K is larger; (ii) component switches induce larger adjacent differences in *logits* $s_{t,j}$; (iii) softmax transfers logit roughness into attention-weight roughness under mild non-degeneracy.

A.1. Setup and assumptions

Mixture of topic labels. Let $K \in \mathbb{N}$ denote the number of mixture components. Each position j has an associated latent topic label

$$c_j \in \{1, \dots, K\}.$$

Assumption A.1 (i.i.d. uniform labels). $(c_j)_{j \geq 1}$ are i.i.d. and $\Pr(c_j = r) = 1/K$ for all $r \in \{1, \dots, K\}$, which means we randomly assign a topic label for the tokens, and each topic has a unique Gaussian distribution. Then, the input token embedding under the view of Gaussian mixture model will follow a GMM: For each j ,

$$x_j = \mu_{c_j} + \varepsilon_j, \quad \varepsilon_j \stackrel{i.i.d.}{\sim} \mathcal{N}(0, \sigma^2 I_d),$$

where $\mu_1, \dots, \mu_K \in \mathbb{R}^d$ are fixed means and $(\varepsilon_j)_j$ are independent of $(c_j)_j$.

Then, if we consider a single-layer causal attention at position t (the position for the next generated token), and Fix $t \geq 2$. Let

$$q_t = W_Q x_t, \quad k_j = W_K x_j, \quad j \leq t-1,$$

and define logits (pre-softmax scores)

$$s_{t,j} = \frac{q_t^\top k_j}{\sqrt{d_q}} = \frac{q_t^\top W_K x_j}{\sqrt{d_q}}, \quad j = 1, \dots, t-1.$$

To simplify the notation system, we further define the induced *score direction* in the input space, where

$$u \triangleq \frac{W_K^\top q_t}{\sqrt{d_q}} \in \mathbb{R}^d, \quad (10)$$

so that

$$s_{t,j} = u^\top x_j. \quad (11)$$

Attention weights from existing token towards next generation token are

$$\alpha_{t,j} = \frac{e^{s_{t,j}}}{\sum_{\ell=1}^{t-1} e^{s_{t,\ell}}}, \quad j = 1, \dots, t-1. \quad (12)$$

Assumption A.2 (Query conditioning). We condition on x_t (equivalently on q_t), and treat u in (10) as deterministic. All expectations below are over $\{(c_j, \varepsilon_j)\}_{j \leq t-1}$.

Separability along the score direction.

Assumption A.3 (Separability). There exists $\Delta > 0$ such that for all $r \neq r'$,

$$|u^\top (\mu_{r'} - \mu_r)| \geq \Delta.$$

In this assumption, we hope that the centroid of Gaussian should be still separable after projection based on W_k and q_t in Equation 10

Softmax non-degeneracy (prevents vanishing pair mass). Fix $j \in \{1, \dots, t-2\}$ and define

$$\Delta s \triangleq s_{t,j+1} - s_{t,j}, \quad m \triangleq \alpha_{t,j} + \alpha_{t,j+1}.$$

Assumption A.4 (Softmax non-degeneracy). There exist constants $\eta \in (0, 1)$, $B \leq 2$, and $\kappa' > 0$, independent of K , such that with

$$E \triangleq \{m \geq \eta\} \cap \{|\Delta s| \leq B\},$$

we have

$$\mathbb{E}[(\Delta s)^2 \mathbf{1}_E] \geq \kappa' \mathbb{E}[(\Delta s)^2].$$

Intuitively, Assumption A.4 says that local logit fluctuations happen in parts of the sequence that the softmax actually “looks at”: with nontrivial frequency, the adjacent pair $(j, j+1)$ receives at least some fixed amount of probability mass, and on those occasions the logit gap is not excessively large. This prevents the situation where logits vary wildly only at positions whose attention weights are almost always zero, in which case attention differences would remain small regardless of logit roughness.

A.2. Sub-claim 1: Adjacent component switching probability increases with K

Lemma A.5 (Switch probability). *Under Assumption A.1, for any $j \geq 1$, the probability of*

$$\Pr(c_{j+1} \neq c_j) = 1 - \frac{1}{K}.$$

Proof. By independence and uniformity,

$$\Pr(c_{j+1} = c_j) = \sum_{r=1}^K \Pr(c_j = r, c_{j+1} = r) = \sum_{r=1}^K \Pr(c_j = r) \Pr(c_{j+1} = r) = \sum_{r=1}^K \frac{1}{K} \cdot \frac{1}{K} = \frac{1}{K}.$$

Taking complements gives $\Pr(c_{j+1} \neq c_j) = 1 - \frac{1}{K}$. □

A.3. Sub-claim 2: Adjacent logit difference energy increases with K

Lemma A.6 (Logit adjacent-difference energy). *Under Assumptions A.1–A.3 and A.2, for any $j \leq t-2$,*

$$\mathbb{E}[(s_{t,j+1} - s_{t,j})^2] \geq 2\sigma^2 \|u\|_2^2 + \left(1 - \frac{1}{K}\right) \Delta^2.$$

Proof. Using (11) and $x_j = \mu_{c_j} + \varepsilon_j$,

$$s_{t,j+1} - s_{t,j} = u^\top (x_{j+1} - x_j) = u^\top (\mu_{c_{j+1}} - \mu_{c_j}) + u^\top (\varepsilon_{j+1} - \varepsilon_j).$$

Let

$$A \triangleq u^\top (\mu_{c_{j+1}} - \mu_{c_j}), \quad B \triangleq u^\top (\varepsilon_{j+1} - \varepsilon_j),$$

so that $s_{t,j+1} - s_{t,j} = A + B$. Then

$$\mathbb{E}[(A + B)^2] = \mathbb{E}[A^2] + 2\mathbb{E}[AB] + \mathbb{E}[B^2].$$

The cross term vanishes: A depends only on topic labels (c_j, c_{j+1}) while B depends only on Gaussian noises $(\varepsilon_j, \varepsilon_{j+1})$, which are independent of labels, and $\mathbb{E}[B \mid c_j, c_{j+1}] = 0$, hence $\mathbb{E}[AB] = 0$.

For the noise term, $\varepsilon_{j+1} - \varepsilon_j \sim \mathcal{N}(0, 2\sigma^2 I_d)$, so

$$B \sim \mathcal{N}(0, 2\sigma^2 \|u\|_2^2) \quad \Rightarrow \quad \mathbb{E}[B^2] = 2\sigma^2 \|u\|_2^2.$$

For the mean-jump term, if $c_{j+1} = c_j$ then $A = 0$. If $c_{j+1} \neq c_j$, Assumption A.3 gives $A^2 \geq \Delta^2$. Therefore

$$\mathbb{E}[A^2] = \mathbb{E}[A^2 \mathbf{1}_{\{c_{j+1} \neq c_j\}}] \geq \Delta^2 \Pr(c_{j+1} \neq c_j) = \Delta^2 \left(1 - \frac{1}{K}\right),$$

where we used Lemma A.5. Combining yields the stated lower bound. □

A.4. Sub-claim 3: Softmax transfers logit roughness to attention roughness

Lemma A.7 (Pairwise softmax difference identity). *Fix t and $j \leq t - 2$. Let $m = \alpha_{t,j} + \alpha_{t,j+1}$ and $\Delta s = s_{t,j+1} - s_{t,j}$. Then*

$$\alpha_{t,j+1} - \alpha_{t,j} = m \tanh\left(\frac{\Delta s}{2}\right).$$

Proof. From (12),

$$\alpha_{t,j+1} - \alpha_{t,j} = \frac{e^{s_{t,j+1}} - e^{s_{t,j}}}{Z}, \quad Z = \sum_{\ell=1}^{t-1} e^{s_{t,\ell}}.$$

Also $m = (e^{s_{t,j+1}} + e^{s_{t,j}})/Z$, hence

$$\alpha_{t,j+1} - \alpha_{t,j} = m \cdot \frac{e^{s_{t,j+1}} - e^{s_{t,j}}}{e^{s_{t,j+1}} + e^{s_{t,j}}} = m \tanh\left(\frac{s_{t,j+1} - s_{t,j}}{2}\right) = m \tanh\left(\frac{\Delta s}{2}\right).$$

□

Lemma A.8 (Softmax transfer lower bound). *Under Assumption A.4 (with $B \leq 2$), for any $j \leq t - 2$,*

$$\mathbb{E}[(\alpha_{t,j+1} - \alpha_{t,j})^2] \geq c \mathbb{E}[(\Delta s)^2], \quad c \triangleq \frac{\eta^2 \kappa'}{16}.$$

Proof. By Lemma A.7,

$$(\alpha_{t,j+1} - \alpha_{t,j})^2 = m^2 \tanh^2\left(\frac{\Delta s}{2}\right).$$

On $\{|\Delta s| \leq B\}$ with $B \leq 2$, we have $|\Delta s|/2 \leq 1$ and use the elementary bound

$$|\tanh(x)| \geq \frac{|x|}{2} \quad \text{for all } |x| \leq 1,$$

which implies $\tanh^2(\Delta s/2) \geq (\Delta s)^2/16$ on $\{|\Delta s| \leq B\}$. On $\{m \geq \eta\}$ we have $m^2 \geq \eta^2$. Therefore on the event

$$E = \{m \geq \eta\} \cap \{|\Delta s| \leq B\},$$

$$(\alpha_{t,j+1} - \alpha_{t,j})^2 \geq \eta^2 \cdot \frac{(\Delta s)^2}{16}.$$

Taking expectations and applying Assumption A.4 yields

$$\mathbb{E}[(\alpha_{t,j+1} - \alpha_{t,j})^2] \geq \frac{\eta^2}{16} \mathbb{E}[(\Delta s)^2 \mathbf{1}_E] \geq \frac{\eta^2 \kappa'}{16} \mathbb{E}[(\Delta s)^2].$$

□

A.5. Main theorem and concise proof via Sub-claims 1–3

Theorem A.9 (Monotone K -dependent lower bound for attention roughness). *Fix $t \geq 2$ and consider the single-layer causal attention row $\alpha_{t,1:t-1}$ defined in (12). Under Assumptions A.1, A.2, A.3, and A.4, there exists a constant $C > 0$ independent of K such that*

$$\mathbb{E}[R_t] \geq C(t-2) \left(1 - \frac{1}{K}\right) \Delta^2.$$

In particular, the right-hand side is monotone increasing in K ; hence $\mathbb{E}[R_t]$ admits a monotone increasing-in- K lower bound.

Proof. By Lemma A.8, for each $j \leq t - 2$,

$$\mathbb{E}[(\alpha_{t,j+1} - \alpha_{t,j})^2] \geq c \mathbb{E}[(s_{t,j+1} - s_{t,j})^2], \quad c = \frac{\eta^2 \kappa'}{16}.$$

Summing over $j = 1, \dots, t - 2$ gives

$$\mathbb{E}[R_t] = \sum_{j=1}^{t-2} \mathbb{E}[(\alpha_{t,j+1} - \alpha_{t,j})^2] \geq c \sum_{j=1}^{t-2} \mathbb{E}[(s_{t,j+1} - s_{t,j})^2].$$

Applying Lemma A.6 yields, for each j ,

$$\mathbb{E}[(s_{t,j+1} - s_{t,j})^2] \geq \left(1 - \frac{1}{K}\right) \Delta^2,$$

where the factor $\left(1 - \frac{1}{K}\right)$ comes from Lemma A.5. Therefore

$$\mathbb{E}[R_t] \geq c \sum_{j=1}^{t-2} \left(1 - \frac{1}{K}\right) \Delta^2 = c(t-2) \left(1 - \frac{1}{K}\right) \Delta^2.$$

Setting $C = c$ completes the proof. \square

A.6. Summary of the logical connection between Sub-claims 1–3

How the pieces fit together. The proof decomposes the K -dependence into three steps:

- (i) **(Sub-claim 1)** Increasing K increases the probability that adjacent inputs come from different mixture components: $\Pr(c_{j+1} \neq c_j) = 1 - \frac{1}{K}$.
- (ii) **(Sub-claim 2)** Under separability along the attention score direction u , a component switch forces a nontrivial expected squared jump in adjacent logits, yielding a lower bound $\mathbb{E}[(s_{t,j+1} - s_{t,j})^2] \geq \left(1 - \frac{1}{K}\right) \Delta^2$ (up to additional noise energy).
- (iii) **(Sub-claim 3)** A pairwise identity for softmax shows $\alpha_{t,j+1} - \alpha_{t,j} = m \tanh(\Delta s/2)$, and under non-degeneracy (m not vanishing too often) this yields $\mathbb{E}[(\alpha_{t,j+1} - \alpha_{t,j})^2] \gtrsim \mathbb{E}[(\Delta s)^2]$.

Chaining (i)–(iii) and summing over j proves Theorem A.9, which provides a monotone increasing-in- K lower bound on $\mathbb{E}[R_t]$.

B. Frequency-aware Operators' Energy Equivalence

In this appendix section, we provide additional technical details on the spectral operators used in our framework and clarify how high-frequency energy can be consistently quantified using the ℓ_2 norm. We show that the Discrete Fourier Transform (DFT), Discrete Wavelet Transform (DWT), and the discrete Laplacian operator all provide principled ways to extract high-frequency components from discrete attention signals, and that their corresponding ℓ_2 norms measure comparable notions of signal energy despite operating in different domains.

B.1. Discrete Fourier Transform

We begin with the DFT, which provides a global frequency-domain representation of discrete signals. Given a token-level attention signal $a_{l,h} \in \mathbb{R}^T$ from layer l and head h , its DFT is defined as

$$\hat{a}_{l,h}(\omega) = \sum_{t=0}^{T-1} a_{l,h}(t) e^{-i2\pi\omega t/T}, \quad \omega = 0, \dots, T-1. \quad (13)$$

A frequency-domain high-pass filter $M(\omega)$ can be applied to isolate high-frequency components, yielding

$$\hat{z}_{l,h}^{\text{hf}}(\omega) = M(\omega) \hat{a}_{l,h}(\omega), \quad (14)$$

where $M(\omega) = 1$ for $\omega \in \Omega_{\text{high}}$ and 0 otherwise. The corresponding high-frequency signal in the token domain is obtained via the inverse DFT.

The use of the ℓ_2 norm as a hallucination score is justified by the *Parseval's theorem* in Section 3.4, which guarantees energy equivalence between the token and frequency domains:

$$\|z_{l,h}^{\text{hf}}\|_2^2 = \frac{1}{T} \sum_{\omega \in \Omega_{\text{high}}} |\hat{a}_{l,h}(\omega)|^2. \quad (15)$$

Thus, the score $s_{l,h} = \|z_{l,h}^{\text{hf}}\|_2$ directly measures the total high-frequency energy of the attention signal, capturing rapid oscillations and global irregularities across the token sequence.

B.2. Discrete Wavelet Transform

DWT provides a multi-resolution analysis of discrete signals, decomposing an attention signal into components at different spatial scales. Using an orthonormal wavelet basis (e.g., Daubechies wavelets), the attention signal $a_{l,h}$ is decomposed into approximation coefficients \mathbf{c}_A and detail coefficients \mathbf{c}_D at multiple scales.

In our framework, the high-frequency component $z_{l,h}^{\text{hf}}$ is reconstructed from \mathbf{c}_D corresponding to fine scales, which capture localized and abrupt changes in attention.

By *Parseval's theorem*, the energy of the attention signal is preserved under an orthonormal wavelet transform, and equals the sum of squared wavelet coefficients. Let $d_{j,k}$ denote the detail coefficient \mathbf{c}_D at scale j and position k . Then,

$$\|z_{l,h}^{\text{hf}}\|_2^2 = \sum_{j \in \mathcal{J}_{\text{high}}} \sum_k |d_{j,k}|^2, \quad (16)$$

where $\mathcal{J}_{\text{high}}$ denotes the set of high-frequency scales.

Accordingly, the score $s_{l,h} = \|z_{l,h}^{\text{hf}}\|_2$ quantifies the localized detail energy of the attention distribution, emphasizing sharp transitions and spatially concentrated irregularities that are characteristic of unstable attention patterns.

B.3. Discrete Laplacian Operator

The discrete Laplacian operator provides a spatial-domain alternative for extracting high-frequency variation. For a one-dimensional attention signal $a_{l,h}$, the discrete Laplacian \mathbf{L} computes second-order differences, measuring how much each token's attention deviates from the average of its immediate neighbors.

The ℓ_2 norm of the Laplacian response,

$$\|\mathbf{L}a_{l,h}\|_2^2, \quad (17)$$

corresponds to the discrete *Dirichlet energy* of the signal, which quantifies its roughness or lack of smoothness (Sandryhaila & Moura, 2014). A higher energy value indicates that the attention distribution exhibits rapid local oscillations or fragmentation, rather than smooth decay or coherent concentration.

The role of the Laplacian as a high-frequency operator can be further understood through its frequency response. In the spectral domain, the discrete Laplacian corresponds to a filter with transfer function

$$H(\omega) = 2 - 2\cos(\omega). \quad (18)$$

As $\omega \rightarrow 0$, $H(\omega) \rightarrow 0$, suppressing low-frequency (smooth) components. As $\omega \rightarrow \pi$, $H(\omega)$ attains its maximum value, strongly amplifying high-frequency components associated with abrupt transitions.

Consequently, the score $s_{l,h} = \|\mathbf{L}a_{l,h}\|_2$ serves as a computationally efficient proxy for high-frequency energy, capturing localized attention instability without requiring an explicit frequency-domain transform.

C. Experiment Details

C.1. Implementation of Baselines

C.1.1. VERIFICATION AND PROBABILISTIC BASELINES

For verification-based baselines, both **SelfCheckGPT** and **RefChecker** use `gpt-4o-mini` as the backbone model for claim extraction and factual verification. For probabilistic consistency baselines, **EigenScore** constructs a similarity matrix

\mathbf{S} based on BERTScore between generated responses, and derives a consistency score from the largest eigenvalue $\lambda_{\max}(\mathbf{S})$. **ReDeEP** computes two complementary signals during generation: an external context score derived from attention allocation over input tokens, and a parametric knowledge score derived from feed-forward network activations, following the original implementation.

Both EigenScore and ReDeEP are strong unsupervised methods specifically designed for hallucination detection that leverage internal model signals, including attention. Despite not being directly trained for the task, they have shown powerful performance and are therefore included as competitive and fair baselines in our comparison.

C.1.2. ATTENTION-BASED FEATURE EXTRACTION

For all intrinsic, attention-based methods (including entropy-based baselines and our frequency-aware features), we extract attention weights from all transformer layers and heads. Let $\mathbf{A} = \{\mathbf{A}_{l,h}\}$ denote the collection of attention distributions, where $\mathbf{A}_{l,h} \in \mathbb{R}^T$ is the token-level attention vector from layer l and head h .

Following (Chuang et al., 2024a), we partition attention into context-directed attention $\mathbf{A}_{l,h}^{(c)}$ and generated-token attention $\mathbf{A}_{l,h}^{(g)}$. For a given head, a feature extraction function $f(\cdot)$ is applied to the corresponding attention distribution. Aggregating across all layers and heads yields separate feature vectors for context and generated attention:

$$\mathbf{v}^{(c)} = [f(\mathbf{A}_{1,1}^{(c)}), \dots, f(\mathbf{A}_{L,H}^{(c)})]^\top, \quad \mathbf{v}^{(g)} = [f(\mathbf{A}_{1,1}^{(g)}), \dots, f(\mathbf{A}_{L,H}^{(g)})]^\top. \quad (19)$$

The final representation is formed by concatenation, $[\mathbf{v}^{(c)}; \mathbf{v}^{(g)}]$, which is then used for hallucination prediction, consistent with the formulation in the main text.

For entropy-based baselines, the feature function $f(\cdot)$ computes the entropy of the attention distribution for each head:

$$H(\mathbf{A}_{l,h}) = - \sum_i a_i \log a_i, \quad (20)$$

where a_i denotes the normalized attention weight assigned to token i .

C.2. Frequency-aware Operators

Discrete Fourier Transform. For DFT, we separate low-frequency and high-frequency components using a frequency cutoff. We systematically vary the cutoff threshold and evaluate hallucination detection performance across models, datasets, and sliding-window settings, as shown in Figure A1. Across most settings, performance improves as the cutoff increases from low values, remains stable over a broad intermediate range, and drops sharply when the cutoff approaches the Nyquist limit.

Here, a normalized frequency of 0.5 corresponds to the Nyquist limit under the DFT formulation. As shown in Figure A1, performance remains stable across a broad range of cutoff frequencies, but begins to degrade when the cutoff exceeds approximately 0.45, with a pronounced drop on the Nyquist boundary. This trend suggests that high-frequency attention variations relevant to hallucination detection are effectively captured below this transition point. Empirically, we find that a cutoff frequency of 0.45 yields consistently strong and stable performance across models and datasets. Additionally, performance is relatively insensitive to lower cutoff settings, with improvements increasing gradually rather than abruptly—indicating robustness to the exact choice of cutoff within a reasonable range.

Discrete Wavelet Transform. For DWT, we perform a multi-resolution decomposition of each attention signal $a_{l,h}$ using the Daubechies-4 (db4) wavelet. The db4 wavelet offers a favorable trade-off between locality and smoothness due to its vanishing moments, making it suitable for capturing abrupt transitions in attention distributions. For boundary handling in finite-length attention sequences, we use zero padding for token-level detection and symmetric padding for span-level detection, based on overall performance observed across datasets and models.

We further compare depth-1 (level1) and depth-2 (level2) wavelet decompositions, as shown in Table A4 and Table A5. Empirically, a depth-1 decomposition consistently outperforms deeper decompositions across datasets and models. We attribute this behavior to the fact that higher-level decompositions increasingly mix lower-frequency components into the detail coefficients, reducing their sensitivity to the finest-scale variations that are most informative for hallucination detection. Accordingly, we adopt a level1 wavelet decomposition in all experiments.

Discrete Laplacian Operator. The discrete Laplacian requires no cutoff or scale selection. Instead, it directly computes second-order differences in the token domain, acting as a local high-pass filter that amplifies rapid attention fluctuations. This simplicity makes the Laplacian operator computationally efficient and parameter-free, while still capturing localized high-frequency variation in attention distributions. As discussed in Appendix B.3, the ℓ_2 norm of the Laplacian response corresponds to the discrete Dirichlet energy, providing a principled measure of attention roughness without additional hyperparameters.

C.3. Model Details

Inference. All experiments are conducted on NVIDIA A100 (80GB) GPUs. The LLMs are kept frozen throughout. We perform inference using teacher-forcing decoding with model response tokens to extract attention distributions for spectral analysis.

Classifiers. Our method uses a lightweight single-layer Logistic Regression classifier. This choice ensures that the detector does not introduce additional non-linear modeling capacity, and that performance differences primarily reflect the discriminative power of the proposed spectral features, rather than classifier expressiveness. The linear detector was implemented using the `scikit-learn` library. All hyperparameters, including the ℓ_2 penalty, were kept at their default values, with the exception of the maximum number of iterations, which was set to 1,000 to ensure model convergence.

Evaluation. For threshold-dependent metrics such as F1, the decision threshold is selected on a held-out validation split and fixed for test evaluation. In cases where an official validation set is not predefined, we reserve 10% of the original training data for this purpose. We use AUROC as our primary metric because AUROC is threshold-independent and is unaffected by this choice.

C.4. Dataset Details

We use two publicly available contextual hallucination detection datasets in this work: RAGTruth and HalluRAG.

Table A1. Statistics of datasets used in our experiments. Length and ratio are calculated on the token level.

Dataset	Task	Train	Val	Test	Prompt Len.	Response Len.	Halluc. Ratio
RagTruth	QA	839	–	150	439.5	208.1	0.1045
	D2T	883	–	150	892.8	225.4	0.0768
	Summ	793	–	150	840.1	153.4	0.0527
HalluRAG	QA	756	162	162	649.3	44.4	0.1530

RAGTruth RAGTruth is a large-scale corpus designed for word-level hallucination detection within retrieval-augmented generation (RAG) frameworks (Niu et al., 2024). It consists of 2,965 manually annotated responses with precise hallucination span labels across three primary tasks: question answering (QA), data-to-text (D2T), and summarization (Summ). The dataset provides standardized train and test splits for each task. Specifically, the QA, D2T, and Summ tasks comprise 839, 883, and 793 training samples, respectively, with each task sharing a consistent test set size of 150 samples.

HalluRAG. HalluRAG focuses on sentence-level hallucination detection in RAG-based QA scenarios (Ridder & Schilling, 2024). It provides generated responses paired with sentence-level annotations, comprising 756 training, 162 validation, and 162 test samples.

More details can be seen in Table A1. All token-level statistics are computed using the tokenizer corresponding to each model, and the reported values are averaged across models. In particular, the hallucination ratio is defined as the number of hallucinated tokens in the response divided by the total number of response tokens. Since this ratio may vary across models, we report the average value over different models.

D. Additional Analysis and Results

This section reports the full experimental results and ablation studies omitted from the main text due to space constraints. These results complement the analyses in the main paper and provide additional details on span-level detection, operator configurations, and the robustness of frequency-aware features across different settings.

D.1. Cross-domain Transfer Analysis

To examine whether the detector captures intrinsic attention-based signals rather than overfits task-specific artifacts, we conduct cross-domain transfer evaluation, where detectors are trained on one task domain and evaluated on another, as shown in Table A2. This experiment also serves to evaluate the generalization ability of the classifier and to test its susceptibility to overfitting.

Table A2. Cross-domain evaluation. Models are trained on the column domain (Source) and evaluated on the row domain (Target). **Bold** values indicate in-domain performance (diagonal, Target=Source). Darker shading corresponds to higher cross-domain performance.

Method	Target	Token-Level (Source)			Span-Level (Source)		
		QA	D2T	Summ	QA	D2T	Summ
Lookback-lens	QA	0.8482	0.7839	0.7741	0.8467	0.8140	0.7985
	D2T	0.6340	0.8442	0.7211	0.6334	0.8551	0.7275
	Summ	0.6618	0.6400	0.7156	0.6563	0.6496	0.6635
Laplacian	QA	0.8449	0.7928	0.7881	0.8365	0.7898	0.7857
	D2T	0.6438	0.8519	0.6809	0.6147	0.8646	0.6264
	Summ	0.6428	0.6678	0.7040	0.6132	0.6596	0.6619
Wavelet-high	QA	0.8526	0.8056	0.8076	0.8680	0.8316	0.8418
	D2T	0.6525	0.8569	0.7179	0.6405	0.8821	0.7307
	Summ	0.6630	0.6773	0.7165	0.6541	0.7032	0.7199
Fourier-high	QA	0.8584	0.8282	0.8233	0.8725	0.8561	0.8593
	D2T	0.6668	0.8595	0.7228	0.6434	0.8869	0.7584
	Summ	0.6781	0.7040	0.7426	0.6748	0.7296	0.7641

Overall, spectral-based detectors exhibit more stable cross-domain behavior compared to Lookback-Lens. In particular, Fourier- and Wavelet-based variants maintain stronger performance when transferring across task boundaries, whereas Lookback-Lens shows larger performance degradation under domain shift. This suggests that frequency-domain attention features capture more task-robust signals than heuristics based on attention mass or recency.

We also observe an asymmetric transfer pattern across tasks. Models trained on QA generally transfer worse to Data-to-Text and Summarization than models trained on Data-to-Text or Summarization transferring to QA. This asymmetry holds consistently across methods and detection granularities. A plausible explanation is that QA exhibits more constrained and localized attention patterns, which may limit the generality of learned aggregation weights when applied to structurally different generation tasks.

D.2. Full Results of Span-level Detection

We report full results for span-level hallucination detection using a sliding-window setting with window size of 8, following the protocol described in the main text. Table A3 presents full performance metrics across models, datasets, and frequency operators.

D.3. Full Results of Ablation Study

This section reports the full results corresponding to the attention-based analyses discussed in the main paper, evaluated across all datasets and models studied.

Figure A2 reports the full results comparing low-pass and high-pass Fourier attention features across all evaluated models, datasets, and both token-level and span-level settings.

Table A3. Full performance comparison on RagTruth and HalluRAG with chunk size set to 8. For each model, the best result is highlighted in **bold**, and the second-best result is underlined.

Model / Method	RT-QA		RT-D2T		RT-Summ		HalluRAG		Overall Avg.	
	F	AUROC	F	AUROC	F	AUROC	F	AUROC	Avg-F	Avg-A
LLaMA-7B										
Lookback-lens	0.7218	0.8467	0.7249	0.8551	0.5852	0.6635	0.6623	0.7856	0.6736	0.7877
Attn-variance	0.5077	0.6979	0.4714	0.5886	0.4840	0.6348	0.4446	0.5209	0.4769	0.6106
Attn-entropy	0.7292	0.8502	0.7060	0.8457	0.5489	0.6637	0.6282	0.6909	0.6531	0.7626
Laplacian	0.7074	0.8365	0.7334	0.8646	0.5833	0.6619	0.6775	0.7754	0.6754	0.7846
Wavelet-high	<u>0.7331</u>	<u>0.8680</u>	0.7478	<u>0.8821</u>	<u>0.6045</u>	<u>0.7199</u>	<u>0.6812</u>	<u>0.7928</u>	<u>0.6917</u>	<u>0.8157</u>
Fourier-high	0.7473	0.8725	<u>0.7348</u>	0.8869	0.6188	0.7641	0.6866	0.8100	0.6969	0.8334
LLaMA-13B										
Lookback-lens	0.7004	0.8594	0.7610	<u>0.8872</u>	0.5728	0.7083	0.7096	<u>0.8505</u>	0.6860	0.8264
Attn-variance	0.5301	0.6871	0.5329	0.7283	0.4917	0.7014	0.5548	0.6412	0.5274	0.6895
Attn-entropy	0.6876	0.8478	0.7226	0.8602	0.5426	0.6377	0.5872	0.6249	0.6350	0.7427
Laplacian	0.6966	0.8467	0.7562	0.8853	<u>0.5930</u>	0.6798	<u>0.7217</u>	0.8264	<u>0.6919</u>	0.8096
Wavelet-high	0.7002	0.8685	0.7225	0.8793	0.5821	<u>0.7202</u>	0.7417	0.8438	<u>0.6866</u>	<u>0.8279</u>
Fourier-high	0.7365	0.8863	0.7706	0.8988	0.6119	0.7904	<u>0.7217</u>	0.8515	0.7102	0.8568
Mistral-7B										
Lookback-lens	<u>0.7920</u>	0.9206	0.7751	0.9002	<u>0.6992</u>	<u>0.8082</u>	0.7752	0.8403	0.7604	0.8673
Attn-variance	0.7036	0.8216	0.6339	0.8112	0.4741	0.6507	0.5709	0.7215	0.5956	0.7512
Attn-entropy	0.7857	0.9007	0.7300	0.8656	0.6606	0.7727	0.6597	0.7140	0.7090	0.8132
Laplacian	0.7500	0.8822	<u>0.7719</u>	<u>0.8928</u>	0.6747	0.7734	0.8056	0.8920	0.7506	0.8601
Wavelet-high	0.7839	0.9083	0.7287	0.8866	0.6771	0.8073	0.7682	0.8802	0.7395	<u>0.8706</u>
Fourier-high	0.8042	<u>0.9190</u>	0.7833	0.9057	0.7114	0.8188	<u>0.7883</u>	<u>0.8872</u>	0.7718	0.8827

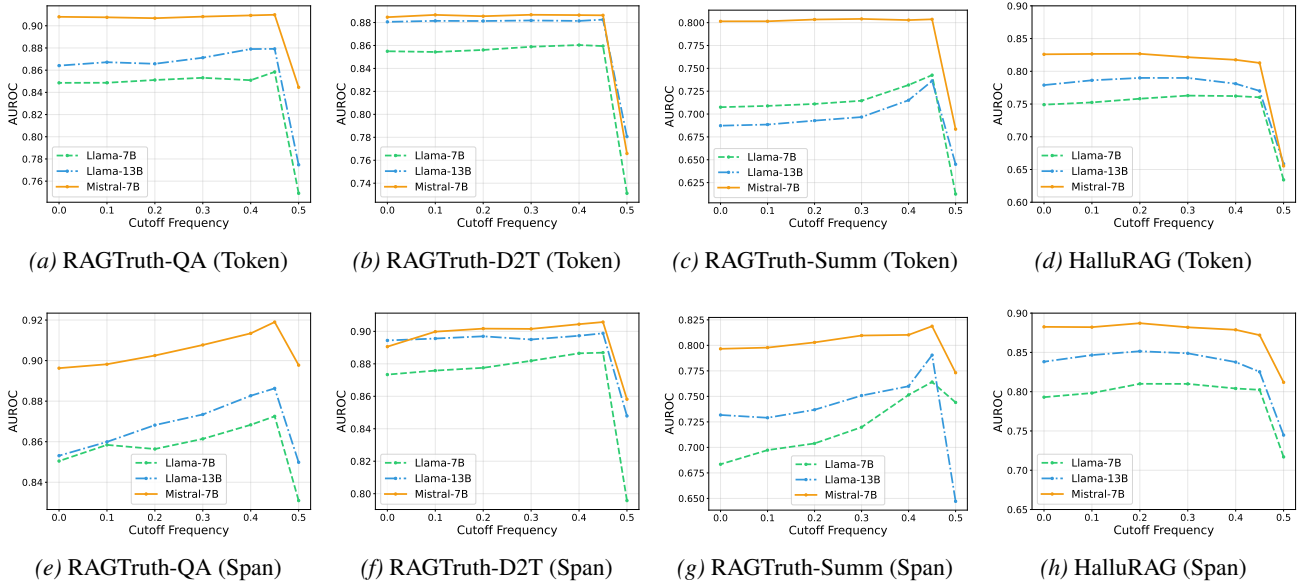


Figure A1. Ablation study on different frequency cutoffs at token and span levels on hallucination detection performance. The top row (a-d) shows results at the token level, while the bottom row (e-h) shows results at the span level.

Detecting Contextual Hallucinations in LLMs with Frequency-Aware Attention

Table A4. Performance comparison on token level using Wavelet-high across levels and padding methods. Best results within each model are in **bold**; second-best are underlined.

Model/Level	Padding	RT-QA		RT-D2T		RT-Summ		HalluRAG		Overall Avg.	
		F	AUROC	F	AUROC	F	AUROC	F	AUROC	Avg-F	Avg-A
LLaMA-7B											
level1	zero	0.7194	0.8526	0.6898	0.8569	0.5929	0.7165	0.6384	0.7550	0.6601	0.7953
	period	<u>0.7146</u>	<u>0.8514</u>	0.6887	0.8517	0.5799	<u>0.7091</u>	0.6360	0.7449	0.6548	0.7893
	symm	0.7215	0.8557	0.6875	<u>0.8545</u>	<u>0.5880</u>	0.7182	0.6353	0.7521	<u>0.6581</u>	<u>0.7951</u>
level2	zero	0.7157	0.8522	<u>0.6893</u>	0.8531	0.5822	0.7088	0.6359	0.7464	0.6558	0.7901
	period	0.7155	0.8514	0.6891	0.8528	0.5814	0.7069	0.6344	0.7438	0.6551	0.7887
	symm	0.7170	0.8519	0.6879	0.8531	0.5851	0.7159	<u>0.6375</u>	<u>0.7543</u>	0.6569	0.7938
LLaMA-13B											
level1	zero	0.7029	0.8741	0.7383	0.8932	0.5651	0.7042	<u>0.6684</u>	<u>0.7809</u>	<u>0.6687</u>	0.8131
	period	0.6962	0.8679	0.7207	0.8811	0.5678	0.7044	0.6527	0.7675	0.6593	0.8052
	symm	<u>0.7002</u>	0.8685	<u>0.7225</u>	0.8793	0.5821	0.7202	0.6718	0.7839	0.6691	<u>0.8130</u>
level2	zero	0.6971	0.8711	0.7213	0.8815	<u>0.5699</u>	0.7043	0.6567	0.7701	0.6613	0.8068
	period	0.6945	0.8675	0.7199	0.8816	<u>0.5687</u>	0.7045	0.6515	0.7669	0.6587	0.8051
	symm	0.6993	0.8701	0.7216	<u>0.8834</u>	0.5678	<u>0.7046</u>	<u>0.6710</u>	0.7789	0.6649	0.8093
Mistral-7B											
level1	zero	0.7876	0.9117	0.7136	0.8829	<u>0.6849</u>	0.8075	<u>0.7274</u>	<u>0.8360</u>	0.7284	<u>0.8595</u>
	period	0.7812	0.9077	0.7228	0.8830	0.6840	0.8034	0.7139	0.8229	0.7255	0.8542
	symm	0.7839	0.9083	0.7287	<u>0.8866</u>	0.6771	<u>0.8073</u>	0.7130	0.8231	0.7257	0.8563
level2	zero	<u>0.7873</u>	<u>0.9113</u>	0.7238	0.8826	0.6844	0.8038	0.7213	0.8265	<u>0.7292</u>	0.8561
	period	<u>0.7770</u>	0.9059	0.7238	0.8826	0.6829	0.8041	0.7130	0.8228	<u>0.7242</u>	0.8539
	symm	0.7831	0.9104	<u>0.7265</u>	0.8869	0.6884	0.8069	0.7308	0.8413	0.7322	0.8614

Figure A3 shows the complete layer-wise importance profiles of frequency-aware attention features across models, including both token-level and span-level detection.

Table A6 presents the full results of the head-level sparsity analysis, reporting detection performance when restricting attention features to the Top- k most important heads across datasets and models.

Table A7 provides the complete ablation results comparing context-only and generated-only attention features for different spectral operators across all evaluation settings.

D.4. Examples of Raw Attention Signals

Figure A4 presents qualitative examples of raw attention distributions from individual attention heads. Each row corresponds to the same attention head at a fixed layer, while the left and right columns show attention over a hallucinated token and a non-hallucinated token, respectively.

We emphasize that these attention distributions reflect real model behavior and are substantially more irregular than the schematic examples shown in Figure 2. In practice, attention weights are often sparse, unevenly distributed, and exhibit non-trivial fluctuations across token positions, rather than forming unimodal patterns (Nawrot et al., 2025).

Notably, for the examples shown in the top row, the two tokens share identical lookback ratios as measured by Lookback-Lens. Similarly, for the bottom row, the context entropy of the two attention distributions is equal. In these cases, these aggregate statistics alone are insufficient to distinguish hallucinated from non-hallucinated cases by visual inspection. In contrast, after applying a high-pass filter to the same attention signals, the resulting high-frequency energy differs substantially between the two cases. Although the raw attention curves may appear similar at a coarse level, frequency-domain filtering reveals differences in fine-grained variation patterns.

Detecting Contextual Hallucinations in LLMs with Frequency-Aware Attention

Table A5. Performance comparison when chunk size is 8 using Wavelet-high across levels and padding methods. Best results within each model are in **bold**; second-best are underlined.

Model/Level	Padding	RT-QA		RT-D2T		RT-Summ		HalluRAG		Overall Avg.	
		F	AUROC	F	AUROC	F	AUROC	F	AUROC	Avg-F	Avg-A
LLaMA-7B											
level1	zero	0.7313	0.8611	0.7479	0.8785	0.6020	0.7169	0.6846	0.8047	0.6915	0.8153
	period	0.7271	0.8572	0.7426	0.8748	0.5973	0.7008	0.6786	0.7963	0.6864	0.8073
	symm	0.7331	0.8680	0.7478	0.8821	<u>0.6045</u>	0.7199	0.6812	0.7928	0.6917	0.8157
level2	zero	0.7277	0.8594	0.7461	0.8760	0.5996	0.6997	0.6800	0.7953	0.6884	0.8076
	period	0.7272	0.8579	0.7452	0.8752	0.5975	0.6972	0.6792	0.7937	0.6873	0.8060
	symm	0.7277	<u>0.8602</u>	<u>0.7478</u>	<u>0.8768</u>	0.6049	<u>0.7107</u>	<u>0.6771</u>	<u>0.7938</u>	<u>0.6894</u>	<u>0.8104</u>
LLaMA-13B											
level1	zero	0.7050	0.8616	0.7833	0.9091	0.5974	0.7557	0.7306	0.8479	0.7041	0.8436
	period	<u>0.7105</u>	0.8610	0.7634	0.8951	0.5984	0.7471	0.7141	0.8338	0.6966	0.8343
	symm	0.7200	0.8718	0.7616	0.8928	0.6043	0.7697	0.7482	0.8541	0.7085	0.8471
level2	zero	0.7079	0.8612	0.7638	0.8953	0.5940	0.7499	0.7168	0.8351	0.6956	0.8354
	period	0.7102	<u>0.8617</u>	0.7637	0.8957	0.5957	0.7485	0.7163	0.8337	0.6965	0.8349
	symm	0.7094	0.8625	<u>0.7664</u>	<u>0.8962</u>	<u>0.5967</u>	<u>0.7563</u>	<u>0.7274</u>	<u>0.8474</u>	<u>0.7000</u>	<u>0.8406</u>
Mistral-7B											
level1	zero	0.7984	0.9111	0.7686	0.9080	0.7010	0.8111	0.7904	0.8777	0.7646	0.8770
	period	0.7858	0.9108	0.7875	0.8997	<u>0.7027</u>	0.8084	0.7900	0.8717	0.7665	0.8726
	symm	<u>0.7970</u>	0.9052	0.7820	0.8995	0.7001	0.8179	<u>0.7921</u>	<u>0.8841</u>	<u>0.7678</u>	0.8767
level2	zero	0.7879	0.9127	<u>0.7887</u>	0.8995	0.7037	0.8096	0.7902	0.8729	0.7676	0.8737
	period	0.7865	0.9116	<u>0.7887</u>	0.8995	0.7023	0.8079	0.7896	0.8727	0.7668	0.8729
	symm	0.7919	<u>0.9074</u>	0.7837	<u>0.9000</u>	0.7035	0.8128	0.8063	0.8876	0.7713	0.8770

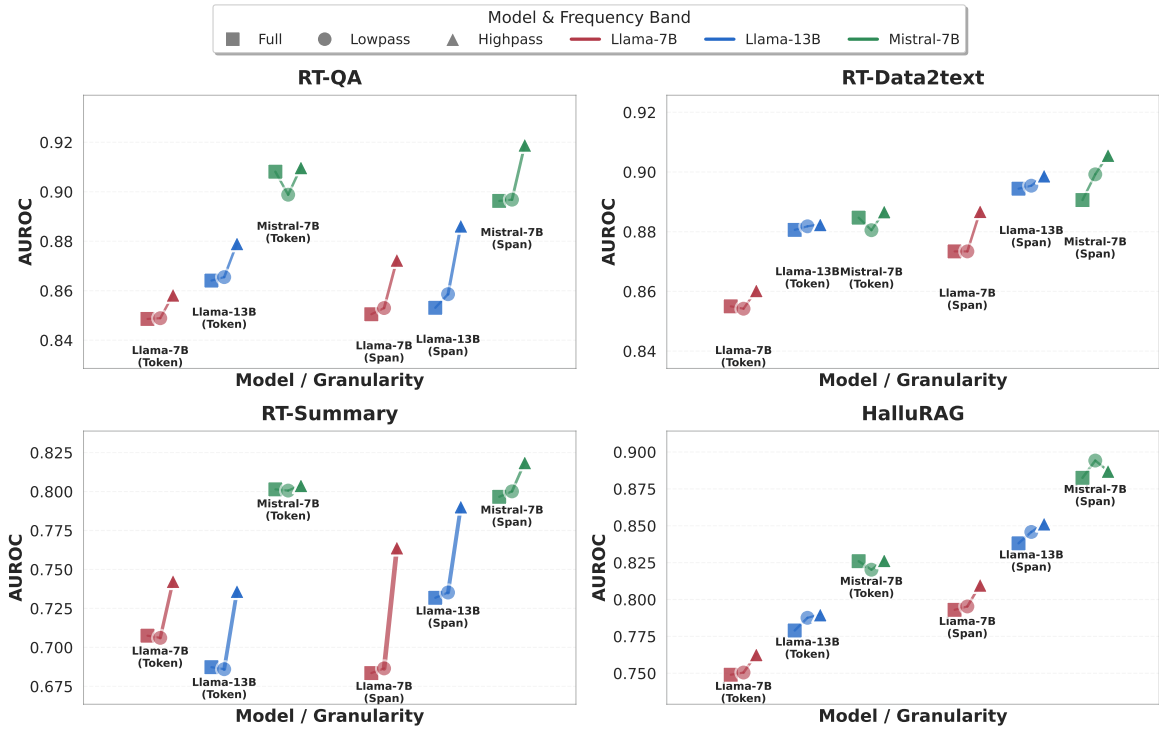


Figure A2. Full results of comparing Full-, Low-, and High-Pass Fourier attention features. Average AUROC across models under token- and span-level evaluation settings.

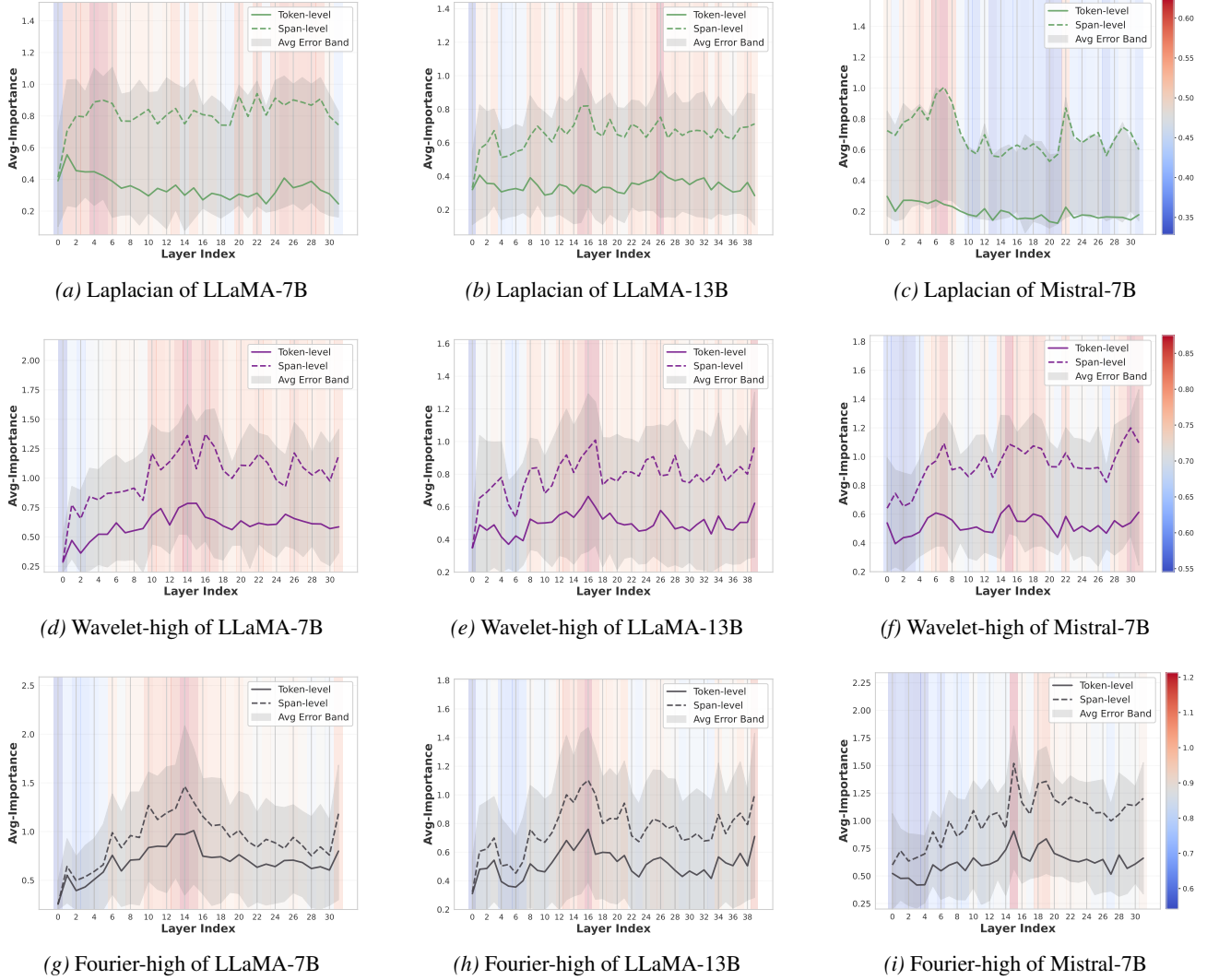


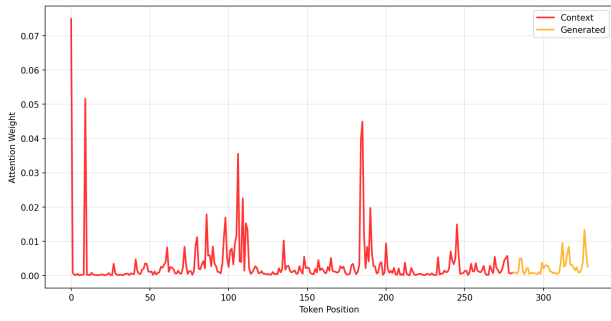
Figure A3. Full results for layer-wise importance. Solid and dashed lines correspond to token-level and span-level detection, respectively. The shaded region indicates the standard deviation of head-level importance within each layer.

Table A6. Original vs. Top- k head only Performance.

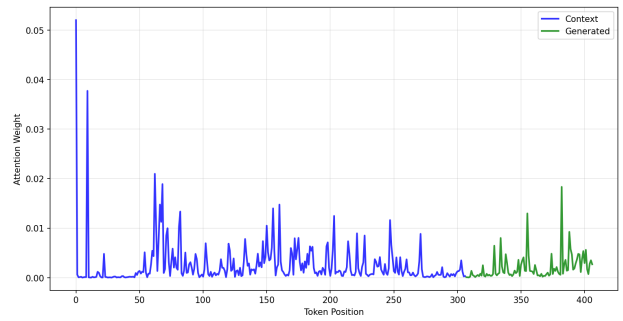
(a) AUROC Results for LLaMA-13B.					(b) AUROC Results for Mistral-7b.				
RagTruth-Avg					RagTruth-Avg				
Method	Original	Top- k heads			Method	Original	Top- k heads		
		$k = 100$	50	10			$k = 100$	50	10
Laplacian	0.8016	0.7858	0.7595	0.6424	Laplacian	0.8625	0.8312	0.7839	0.6795
Wavelet-high	0.8238	0.8079	0.7821	0.7191	Wavelet-high	0.8673	0.8483	0.8317	0.7707
Fourier	0.8326	0.8204	0.7899	0.7041	Fourier-high	0.8669	0.8440	0.8283	0.7624
HalluRAG					HalluRAG				
Method	Original	Top- k heads			Method	Original	Top- k heads		
		$k = 100$	50	10			$k = 100$	50	10
Laplacian	0.7624	0.6924	0.6764	0.6335	Laplacian	0.8098	0.7611	0.7433	0.6807
Wavelet-high	0.7809	0.7433	0.7133	0.6292	Wavelet-high	0.8360	0.7715	0.7467	0.7091
Fourier-high	0.7899	0.7749	0.7572	0.6455	Fourier-high	0.8267	0.7855	0.7587	0.6920

Table A7. Ablation study comparing context-only and generated-only attention features. Results are reported across spectral operators and models.

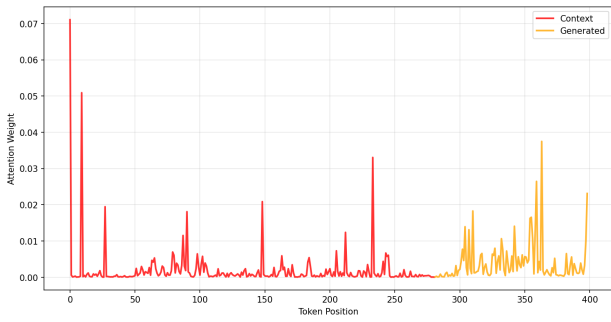
Model	Setting	Operator	RagTruth-Avg		HalluRAG	
			F	AUROC	F	AUROC
LLaMA-7B	Original	Laplacian	0.6588	0.8003	0.6370	0.7429
		Wavelet-high	0.6673	0.8087	0.6384	0.7550
		Fourier-high	0.6685	0.8205	0.6478	0.7629
	Context-only	Laplacian	0.6504	0.8014	0.6340	0.7396
		Wavelet-high	0.6541	0.8074	0.6402	0.7479
		Fourier-high	0.6544	0.8138	0.6385	0.7538
	Generated-only	Laplacian	0.6441	0.7855	0.6183	0.7240
		Wavelet-high	0.6430	0.7889	0.6264	0.7334
		Fourier-high	0.6416	0.7939	0.6262	0.7349
LLaMA-13B	Original	Laplacian	0.6526	0.8016	0.6659	0.7624
		Wavelet-high	0.6688	0.8238	0.6684	0.7809
		Fourier-high	0.6759	0.8326	0.6732	0.7899
	Context-only	Laplacian	0.6603	0.8144	0.6538	0.7627
		Wavelet-high	0.6634	0.8206	0.6524	0.7697
		Fourier-high	0.6688	0.8333	0.6581	0.7815
	Generated-only	Laplacian	0.6468	0.7988	0.6430	0.7503
		Wavelet-high	0.6579	0.8080	0.6524	0.7697
		Fourier-high	0.6446	0.8053	0.6473	0.7642
Mistral-7B	Original	Laplacian	0.7262	0.8625	0.7001	0.8098
		Wavelet-high	0.7287	0.8673	0.7274	0.8360
		Fourier-high	0.7300	0.8669	0.7221	0.8267
	Context-only	Laplacian	0.7289	0.8636	0.7207	0.8242
		Wavelet-high	0.7280	0.8655	0.7176	0.8238
		Fourier-high	0.7299	0.8668	0.7128	0.8227
	Generated-only	Laplacian	0.7151	0.8515	0.6840	0.7802
		Wavelet-high	0.7185	0.8548	0.6994	0.7983
		Fourier-high	0.7178	0.8531	0.6895	0.7913



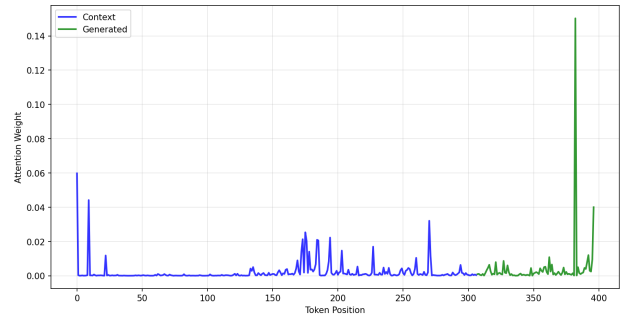
(a) Layer 13, Head 09: Attention for a hallucinated token



(b) Layer 13, Head 09: Attention for a non-hallucinated token



(c) Layer 15, Head 29: Attention for a hallucinated token



(d) Layer 15, Head 29: Attention for a non-hallucinated token

Figure A4. Raw attention signal visualizations. Each subfigure compares raw attention distributions for a hallucinated token (left) and a non-hallucinated token (right). Red and yellow curves denote attention over context and generated tokens, respectively, when generating a hallucinated token, while blue and green curves denote attention over context and generated tokens for a non-hallucinated token.